



# WBM: A scalable gridded global hydrologic model with water tracking functionality

Danielle S. Grogan<sup>1</sup>, Shan Zuidema<sup>1</sup>, Alex Prusevich<sup>1</sup>, Wilfred M. Wollheim<sup>1,2</sup>, Stanley Glidden<sup>1</sup>, Richard B. Lammers<sup>1</sup>

5 <sup>1</sup>Earth Systems Research Center, Institute for the Study of Earth, Oceans, and Space, University of New Hampshire, Durham, NH, 03824, US

<sup>2</sup>Department of Natural Resources and the Environment, University of New Hampshire, NH, 03824, USA

Correspondence to: Danielle S. Grogan ([danielle.grogan@unh.edu](mailto:danielle.grogan@unh.edu)) and Shan Zuidema ([shan.zuidema@unh.edu](mailto:shan.zuidema@unh.edu))

**Abstract.** This paper describes the University of New Hampshire Water Balance Model, WBM, a process-based gridded  
10 global hydrologic model that simulates the land surface components of the global water cycle and includes water extraction for use in agriculture and domestic sectors. WBM has a long publication history; here we describe the first fully open source WBM version. This version includes a suite of water source tracking modules that enable analysis of flow-path histories on water supply. Earlier descriptions of WBM methods provide the foundation of the most recent model version detailed here. WBM is available here: <https://github.com/wsag/WBM>. WBM is written in the perl data programming language (PDL),  
15 making use of several open-source perl libraries. As a convenience we also provide a Singularity container that simplifies installation of dependencies. We present an overview of the model functionality, utility, and validation of global river discharge and irrigation water use using data from the Global Runoff Data Centre and FAO statistics. A key feature of WBM is the ability to identify the partitioning of sources for each stock or flux within the model. Therefore, users can determine what proportion of any flux consists of each of the primary inputs of water to the surface of the terrestrial hydrologic cycle,  
20 previously extracted water for human uses, or runoff generated from any place on the Earth's surface. Such component tracking provides both a more fully transparent model in that users can identify the underlying mechanisms generating the simulated behavior, as well as perform model experiments in new ways.

## 1 Introduction

Global hydrologic models (GHMs) are one of the primary tools used in the study of macro-scale hydrology, and the past 30  
25 years has seen the development of numerous GHMs. These include WBM (Vörösmarty et al. 1989), VIC (Liang et al. 1994), WaterGAP (Döll et al. 2003), H08 (N. Hanasaki et al., 2008a, 2008b), PCR-GLOBWB (Sutanudjaja et al., 2018), and others (Telteu et al., 2021). The terrestrial hydrology concepts and structures from these models have now been incorporated into several land surface models (LSMs), e.g., NASA LIS (Kumar et al., 2006), and Earth system models (ESMs) such as the Community Land Model (CLM; Lawrence et al., 2019) and WRF-Hydro (Gochis et al., 2020), and others such as the U.S.  
30 National Water Model (Cohen et al., 2018). GHMs represent the land surface component of the hydrologic cycle, converting



time series of weather and landcover variables into estimates of water storage and flux values. These models have been applied to many questions of both basic and applied hydrology, such as climate change and other anthropogenic impacts on global river systems (Bosmans et al., 2017; Döll et al., 2012; Haddeland et al., 2014; Hanasaki et al., 2008b; Vörösmarty et al., 2000a, 2010; Wada et al., 2011), groundwater depletion (Petra Döll et al., 2014; Gleeson et al., 2012; Grogan et al., 2017; Wada et al., 2012), and the role of water extractions in sea level change (Gleeson et al., 2012; Konikow, 2011; Pokhrel et al., 2012). GHMs have also been used extensively in the study of food security and agricultural yields (Biemans & Siderius, 2019; Döll & Siebert, 2002; Elliott et al., 2014; Haqiqi et al., 2020; Liu et al., 2017; Schewe et al., 2014) as well as formed the foundation for water quality models (Mineau et al., 2015; Stewart et al., 2011a; Wit, 2001; Wollheim et al., 2008a,b; Zuidema et al., 2018) and the inputs for flood inundation models (e.g., Yamazaki et al., 2011). Recently, GHMs have been employed in interdisciplinary studies to evaluate human-hydrologic systems and the food-energy-water nexus, e.g., human and economic impacts of flooding (Dottori et al., 2018), hydropower (Mishra et al., 2020; Turner et al., 2019) and powerplant cooling capacity (van Beek et al., 2012; Stewart et al., 2013; Webster et al., 2022), water markets (Rimsaite, 2021), irrigation decision-making under climate change (Zaveri et al., 2016), and virtual water trade (Dalin et al., 2017; Konar et al., 2013). A recent overview of GHM literature is also provided in Sutanudjaja et al. (2018).

## 1.1 Tracking water sources

As pressures on water resources increase through both climate change and intensifying human water demand (e.g., Vörösmarty et al., 2000a), it is important to know the origin of regional water resources. While some basins may be supplied by steady precipitation or recharging aquifers, others rely on seasonal snowpack, fossil groundwater, irrigation returns, glacial melt, or monsoon rains. Each of these water sources comes with their own set of management challenges and opportunities, making knowledge of water sources a vital component of water resource planning. It may seem obvious where a basin or region's water comes from; however, human water use introduces complexities into the terrestrial water cycle that can obscure the often lengthy and circuitous pathway that waters take from source to use (Grogan et al., 2017; Zuidema et al., 2020). Under natural conditions, most of the water that enters a river basin travels from the land surface through soils and groundwater to headwater basins (Alexander et al., 2007) and then through the full river system to the ocean or endorheic outlet. Humans withdraw large quantities of water from these natural pathways; no human water use activity is completely consumptive, causing some water that is extracted from river and groundwater systems to be either returned to its original source or diverted to an alternate pool. Irrigation accounts for ~70% of all freshwater withdrawals (Rosegrant & Cai, 2002), and globally is ~50% efficient (Döll & Siebert, 2002; Gleick et al., 1993), returning approximately half of all extracted water back to the system. The repetition of this activity causes iterative cycles of water extraction and return, creating complex, circuitous pathways. The pathways that water travels impact water quality (Huang et al., 2022; Mineau et al., 2015), food security (Kadiresan & Khanal, 2018), and governance of water resources through transboundary interactions (Zeitoun & Mirumachi, 2008). Furthermore, humans



develop hydro-infrastructure to intentionally impound (Lehner et al., 2011; Zuidema & Morrison, 2020) and divert rivers (Ghassemi & White, 2007), and engage in artificial recharge of groundwater pools (Dillon et al., 2019). These activities divert water through natural and artificial stocks, masking the identity of the original source of the water.

Understanding the journey of certain sources of water illuminates their role in downstream water resource issues and how human-induced complex pathways make attribution of upstream changes to downstream effects increasingly difficult. In this paper we present three examples of tracking parcels of water through the hydrological cycle by preserving key attributes related to water sources, return flows from water extraction, and land and an identifier assigned to all runoff generated from a given land area. This novel modeling method maintains the identity of a parcel of water as it travels through natural and anthropogenic pathways, illuminating previously obscured connections between sources, uses and fates, as well as offering a potential useful tool for understanding water quality changes throughout watersheds.

## 2 WBM model description

### 2.1 General overview

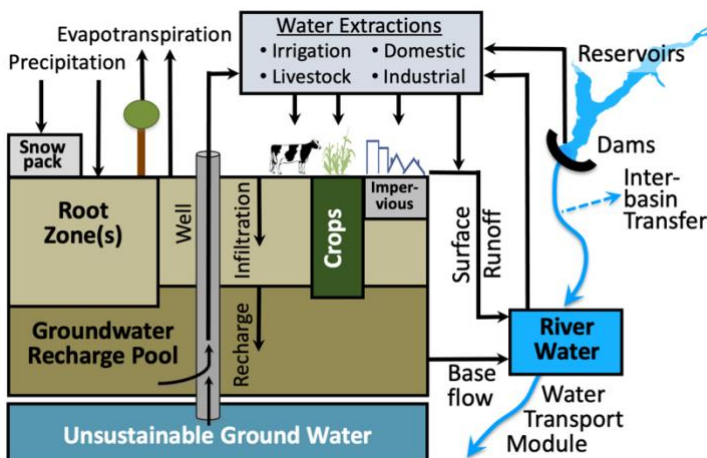


**Figure 1.** Water balance model schematic showing major fluxes and storages.

WBM (Grogan, 2016; Wisser et al., 2010a) is a process-based, gridded hydrologic model that simulates spatially and temporally varying water volumes and quality (Fig. 1). It was one of the first GHMs developed (Vörösmarty et al., 1989), and is now joined by many other similar GHMs and LSMs in its representation of the terrestrial portion of the water cycle. WBM represents all major land surface components of the hydrologic cycle, and tracks fluxes and balances between the atmosphere, above-ground water storages (e.g. snowpack), soil, vegetation, groundwater, and runoff. A digitized river



network connects each grid cell to the next, enabling simulation of flow through river systems. WBM includes domestic and industrial water requirements and use, agricultural water requirements and use (irrigation and livestock), and hydro-  
85 infrastructure (dams and inter-basin transfers). While the model is considered global, it can be run for any region and any spatial resolution given available input data at the appropriate scale. For example, WBM has been operated at a local scale of 120-meter grid cell resolution over a 400 km<sup>2</sup> watershed (Stewart et al., 2011a), and at global scales (Grogan et al., 2017; Wisser et al., 2010a) (Table 1).

90 WBM is modular and is able to accept climate, land use/land cover, water management, and water demand inputs from other models and data sources, such as glacier melt models (e.g., (Huss & Hock, 2015; Rounce et al., 2020)), reservoir operation data (Zuidema et al., 2020), or econometric land use models (Zaveri et al., 2016). In contexts where water quality is simulated, fluxes of solutes from other models such as the terrestrial biogeochemical model PnET (Aber et al., 1997) provide the relevant boundary conditions to WBM (Samal et al., 2017). While WBM is modular, the core hydrologic framing  
95 requires the following inputs: a digital river network identifying flow direction at the resolution of the model grid (e.g., STN-30p (Vörösmarty et al., 2000b), MERIT (Eilander et al., 2021; Yamazaki et al., 2019), HydroSHEDS (Lehner et al., 2008), or any other standard flow grids); soil available water capacity and root depth; daily average temperature, and total daily precipitation. Model methods and results described here specifically refer to the open source release of WBM, WBM v1.0.0 (Grogan and Zuidema, 2022).

100

**Table 1.** Examples of WBM applications over different regions across the globe.

Region	Citations
Global	Fekete et al., 2006; Grogan, 2016; Grogan et al., 2017; Liu et al., 2017; Schewe et al., 2014; Vörösmarty et al., 2000a, 2010; Wisser et al., 2008; Wisser et al., 2010a,b
Arctic	Bring et al., 2017; Rawlins et al., 2003, 2005, 2019; Rawlins et al., 2006a,b; Shiklomanov et al., 2013
Asia	Douglas et al., 2006; Grogan et al., 2015; Groisman et al., 2020; Mishra et al., 2020; Zaveri et al., 2016
Africa	Vörösmarty et al., 2005
South America	D’Almeida et al., 2006; Vörösmarty et al., 1989
North America	Grogan et al., 2020; Rougé et al., 2021; Samal et al., 2017; Stewart et al., 2011b, 2013; Vörösmarty et al., 1998; Webster et al., 2022; Zuidema et al., 2018, 2020
Tropics	Douglas et al., 2005; Douglas et al., 2006



Most features of WBM have been described in prior publications, and the documentation included in the WBM GitHub repository provides details and equations for all the WBM v1.0.0 model methods. Here, we give a general overview, describe updates and additions to previously published methods, and point to the most recent and relevant citations where they accurately describe the version of the model presented here.

## 2.2 Model description

### 2.2.1 Land surface fluxes

Water enters the land surface – and therefore enters the WBM modelling framework – via precipitation. This precipitation can be intercepted by the vegetative canopy, collect as snow, enter soil storage, or become surface runoff. Water that enters soils in excess of the soil’s field capacity infiltrates into the shallow groundwater pool. Bare surfaces and vegetation collectively lose water to the atmosphere through evapotranspiration.

*Precipitation and snow:* Precipitation is partitioned into solid (snow) and liquid (rain) within WBM according to temperature thresholds. Snow accumulation and melt, both expressed in terms of snow water equivalent (SWE), are also functions of temperature thresholds. These snow thresholds are fully described in (Wada et al., 2012) and (D. S. Grogan, 2016). For regions with high elevational gradients, a sub-grid cell binned distribution of elevations can be used to partition the grid into liquid/solid precipitation portions and snow accumulation/melt portions. If sub-grid elevation snow processes are not used, the same snow processes apply to the entire grid cell. The sub-grid cell elevation method described in (Mishra et al., 2020) and (D. S. Grogan et al., 2020) is elaborated on here. The elevation distribution of each model grid cell is calculated from a 30-meter or finer resolution digital elevation model (DEM), resulting in binned elevation categories of  $\Delta H$  vertical bands. The size of the bins is user-defined and can be from 0 to 5000 meters, with a default bin  $\Delta H$  size of 250 meters. A temperature lapse rate,  $L$  [ $^{\circ}\text{C}/\text{km}$ ], is applied to the mean daily temperature,  $T$  [ $^{\circ}\text{C}$ ] at the reference elevation,  $H_{ref}$  [m] for each binned elevation category, resulting in an adjusted mean temperature,  $T_e$  [ $^{\circ}\text{C}$ ], for the portion of each grid cell in elevation bin category  $e$ .

$$T_e = T + \frac{L}{1000} (H_e - H_{ref}) \quad (1)$$

The reference elevation,  $H_{ref}$  [m], is the average elevation of the grid cell represented by the temperature dataset. Precipitation rates are assumed to be equal across all elevation bins  $e$ , such that  $P^e = P$ , where  $P^e$  is the precipitation rate at elevation  $e$  [mm/day], and  $P$  is the input precipitation rate [mm/day]. Snow water equivalent (SWE) is updated through timesteps of length  $dt$  in elevation bin  $e$  as:

$$\frac{dS^e}{dt} = P_s^e - M^e \quad (2)$$



Where the frozen precipitation rate,  $P_s^e$  [mm/d] is defined by comparing the temperature at elevation  $e$ ,  $T^e$  [°C], to a reference temperature  $T_s$  [°C]:

$$135 \quad P_s^e = \begin{cases} P & \text{if } T^e < T_s \\ 0 & \text{if } T_s \leq T^e \end{cases} \quad (3)$$

and snowmelt at elevation bin  $e$ ,  $M^e$ , [mm/d] is defined according to (Willmott et al., 1985):

$$M^e = \begin{cases} 2.63 + 2.55 T^e + 0.0912 T^e P & \text{if } T_m < T^e \\ 0 & \text{if } T^e \leq T_m \end{cases} \quad (4)$$

Total SWE,  $S$ , [mm/d] in the grid cell at each time-step is the sum of all SWE values at each elevation band  $e$  multiplied by the corresponding fraction of grid cell area represented by elevation bin  $e$ ,  $f^e$ :

$$140 \quad S = \sum_{e=1}^n S^e f^e \quad (5)$$

Variables controlling SWE accumulation include the snowfall threshold  $T_s$ , with a default value of -1 °C; the snow melt threshold  $T_m$ , with a default value of 1 °C; and  $L$  is the lapse rate, with a default value of -6.4 °C/km. Both  $T^e$  and  $L$  can be constants for the whole simulation domain, or they can be a spatially variable gridded input layer.

145 At high elevations and cold climates, it is a common case that annual snowfall exceeds annual snowmelt volume. In reality, this excess snowpack converts to ice and forms glaciers. WBM does not internally simulate glacier formation or dynamics; this causes unrealistic, infinite snow accumulation. To address this problem, users can define a threshold (e.g., 5000 mm of snow water equivalent) above which snow water volumes are shifted down elevation bands on the date of annual snowpack minimum (assumed to be August 15 in the Northern hemisphere and February 15 in the Southern hemisphere). If there is no  
 150 elevation bin in the grid cell in which snow is melting, snow water is further shifted downstream to the next grid cell, following the direction of flow as defined by the digital river network.

*Canopy interception:* Vegetation intercepts incoming precipitation, preventing some of the total precipitation from reaching soils below and adding to the total evapotranspiration flux. The canopy intercepts liquid precipitation only. WBM uses canopy  
 155 rain interception formulations from (Deardorff, 1978) and (Dickinson, 1984), which calculates the canopy water balance as:

$$\frac{dW_i}{dt} = (P - P_t) - E_c, \quad \text{where } W_i \leq W_i^{max} \quad (6)$$

where  $W_i$  is canopy water storage [mm],  $P$  and  $P_t$  are liquid precipitation and throughfall respectively [mm/d],  $E_c$  is evaporation of the canopy water [mm/d].

160 Canopy water storage is limited by its capacity  $W_i^{max}$  which is proportional to the Leaf Area Index (LAI) [m<sup>2</sup>/m<sup>2</sup>]

$$W_i^{max} = C_{LAI} * LAI \quad (7)$$



where  $C_{LAI}$  is canopy interception coefficient [mm], which typically ranges from 0.15 to 0.25 mm (Dingman, 2002); WBM uses a default value of 0.2 mm, as suggested in (Dickinson, 1984).

165 The canopy water evaporation rate  $E_c$  [mm/d] is estimated as a simplification of the relation given by (Deardorff, 1978):

$$E_c = E_{ow} * \left( \frac{W_i}{W_i^{max}} \right)^{2/3} \quad (8)$$

Throughfall is then calculated as the amount of water over-filling the canopy interception pool, while accounting for evaporation over the course of the time-step.

170 *Open water and Impervious surfaces:* WBM represents direct storm runoff over impervious surfaces (Zuidema et al., 2018), which prevents water from entering soil and increases storm runoff. If provided with a map of impervious surface fraction of grid cell area, WBM assumes no soil water holding capacity and does not calculate canopy interception on those areas. To define the fraction of precipitation that is routed directly to streams, WBM calculates an effective impervious area adapted from (Alley & Veenhuis, 1983):

$$175 \quad f_{imp}^{eff} = f_{imp}^{0.4} \quad (9)$$

Given an input dataset of the fraction of grid cell open water,  $f_{ow}$ , areas (e.g., lakes and ponds), WBM treats open water areas as direct contributors of storm runoff to river systems, e.g., they have no soil infiltration, surface retention pool, or shallow groundwater pool. WBM limits the sum of impervious surface and open water areas to 97.5% of grid cell area for continuity, except for expansive lakes occupying entire grid cells which are masked from any terrestrial water balance calculations. Direct

180 storm runoff,  $R_{strm}$  [mm/d], is calculated as the sum of incoming precipitation,  $P$  [mm/day], and snow melt water,  $M$  [mm/day], multiplied by the sum of the effective impervious area fraction,  $f_{imp}^{eff}$ , and open water fraction,  $f_{ow}$ :

$$R_{strm} = (f_{imp}^{eff} + f_{ow})(P + M) \quad (10)$$

Storm runoff,  $R_{strm}$  [mm/d], is routed directly to streams. The remainder of precipitation and snowmelt water are routed to soil infiltration.

185

*Soil moisture balance:* Soil moisture balance,  $W_s$  [mm], is calculated with an accounting system that tracks a grid cell's water inputs, water outputs, and soil moisture pool holding capacity. The soil moisture pool depth is determined by the rooting depth. Inputs come in the form of throughfall of liquid precipitation,  $P_t$  [mm/d], and as snow melt,  $M$  [mm/d]. Output is via actual evapotranspiration,  $AET$  [mm/d], modified by a soil drying function,  $g(W_s)$ , and gravity drainage  $D$  [mm/d]. Soil moisture balance calculations for natural landcovers are fully described in (Wisser et al., 2010a) and crop landcovers in (Grogan, 2016).

190

*Potential and actual evapotranspiration:* Evaluation of different potential evapotranspiration (PET) functions is provided in (Vörösmarty et al., 1998); the version of WBM described here has options to use the Hamon (1963), Penman-Monteith



195 (Penman, 1948; Monteith, 1965), and FAO Drainage Paper No. 56 modification to Penman-Monteith (Allen et al. 1998) PET functions. The Hamon method requires only two climate inputs (temperature and precipitation), while the other two functions require additional inputs of air humidity (relative, absolute, or dew/wet bulb temperature), wind speed vectors, and cloud cover. The Hamon and Penman-Monteith functions are both described in (Vörösmarty et al., 1998), and the FAO Drainage Paper No. 56 (Allen et al., 1998) modification to Penman-Monteith PET is described in the WBM model documentation provided on GitHub (<https://github.com/wsag/WBM/tree/main/documentation>).

200

Actual evapotranspiration (AET) from naturally vegetated land areas is a function of the PET, soil moisture, and soil properties. If soil moisture is sufficient, then  $AET = PET$ . Otherwise, PET is modified by a soil drying function,  $g(W_s)$ . The amount of water that can be drawn out of the soil moisture pool depends on the current soil moisture and the available water capacity. These functions are described fully in Wissler et al. (2010a) and Grogan (2016). Evapotranspiration from land cover types other than a generic natural land can be represented, given input data on the sub-grid cell fraction occupied by these land cover types and a set of associated parameters. When using sub-grid cell land cover inputs, WBM simulates a full water balance for each portion of the grid cell identified as a unique land cover type. Model output provides a grid-averaged value for each stock and flux. For cropland land cover inputs, sub-grid cell crop-specific water balance values can be output for soil moisture, PET, irrigation water applied (for irrigated crops), and blue water and green water use by crop (for irrigated crops). For fine resolution simulations, inputs identifying the dominant land cover type can be used to parameterize the entire grid cell, or land-cover can be used to average necessary parameters *a priori*. Crop ET calculation methods are from (Allen et al., 1998), with Default parameter values for crops from (Siebert & Döll, 2010). While AET from other land cover types (e.g., forest or grassland) can be parameterized and simulated, no published study has yet used this option of WBM. Actual evapotranspiration from other consumptive water uses are described below in Section 2.2.5.

215

Open water evaporation applies to the fraction of grid cells containing terrestrial free water surfaces, including river surface area, lake and reservoir area, and inter-basin transfer canal area (see 2.3.4 below for a description of inter-basin transfer canals). Open water evaporation rates can be input to WBM, available from reanalysis models like MERRA2 (Gelaro et al., 2017), or estimated as a multiplier on PET in the absence of an input dataset; the default multiplier in WBM is 1.0. The river surface evaporation,  $E_{riv}$ , is calculated as a function of open water evaporation rates,  $O$ , and river geometry:

220

$$E_{riv} = \min(\sqrt{A} \cdot y_r E_{ow}, W_R), \quad (11)$$

where  $A$  is the grid cell area [ $m^2$ ],  $y_r$  is the stream width [ $m$ ],  $E_{ow}$  is the open water evaporation rate [ $m/day$ ], and  $W_r$  is the storage of water in the river [ $m^3$ ]. Hydraulic geometry relations used to estimate stream width are described below in Section 2.2.3.

225

*Surface runoff*: When water enters a grid cell in excess of the volume that can be stored in soils, the canopy, and lost through evapotranspiration, then gravity drainage occurs resulting in both surface runoff and recharge. The distribution of this excess





230 water between surface runoff and shallow groundwater recharge is defined by a model parameter which sets the fraction of drainage water that recharges shallow groundwater; the complement of this value is treated as surface runoff. To capture the hydrodynamic response of runoff generation following precipitation and melt events, water passes through either a surface retention pool or a shallow groundwater pool, described below.

235 Surface runoff,  $R_S$  [mm/day], is retained in the surface runoff retention pool,  $W_{SRP}$  [mm], prior to draining to the stream network. This temporary storage of surface runoff in the surface retention pool represents flow over the land-surface and temporary storage in ephemeral pools and wetlands. The drainage rate,  $R_{SRP}$ , [mm/day] from the surface runoff retention pool,  $W_{SRP}$  [mm], follows a tank drainage formulation:

$$R_{SRP} = C_{SRP} \sqrt{2 G W_{SRP}} \quad (12)$$

Where  $C_{SRP}$  is a unitless discharge coefficient of the surface runoff retention pool and includes unit conversions, and  $G$  is gravitational acceleration.

240 There is an upper limit,  $T_{SRP}$  [mm], imposed on the storage volume in the surface runoff retention pool. This limit captures the response of over-filled surface topographic depressions. When the volume of the surface runoff retention pool exceeds this limit, then the over-flow water,  $R_{EXC}$  [mm/day], is immediately moved to the river. This helps to capture flashy hydrodynamic responses more accurately during extreme events (Zuidema et al., 2020). Change to the storage value of the surface runoff retention pool  $W_{SRP}$  is:

$$\frac{dW_{SRP}}{dt} = R_S - R_{SRP} - R_{EXC} \quad (13)$$

where  $R_S$  [mm/day] is surface runoff,  $R_{SRP}$  [mm/day] is the drainage rate out of the surface runoff retention pool, and  $R_{EXC}$  [mm/day] is the over-flow water.

The balance of the surface runoff retention pool is calculated as a split operator in three stages:

250 1.  $W_{SRP}^1 = W_{SRP}^k + R_S$  (14)

2.  $W_{SRP}^2 = W_{SRP}^1 - R_{SRP}$  (15)

where  $R_{SRP} = C_{SRP} \sqrt{2 G W_{SRP}^1}$  (16)

3.  $W_{SRP}^{k+1} = W_{SRP}^2 - R_{EXC}$  (17)

255 where  $R_{EXC} = \begin{cases} T_{SRP} - W_{SRP}^2 & \text{if } W_{SRP}^2 > T_{SRP} \\ 0 & \text{if } W_{SRP}^2 \leq T_{SRP} \end{cases}$  (18)

Where  $W_{SRP}^k$  and  $W_{SRP}^{k+1}$  are the storage in the surface retention storage pool at the previous and present time-step, respectively. The threshold for storage in the surface runoff retention pool ( $T_{SRP}$ ) is set to 1000 mm by default, which effectively turns off



this functionality unless an alternate value is defined. Decreasing  $T_{SRP}$  to values in the range of 15 to 50 mm increase the flashy response of the model in temperate climates.

260

*Glacier runoff:* Another flux of water from the land surface to the rivers is glacier runoff. While WBM does not simulate glacier formation and dynamics, it can take inputs of glacier area and runoff generated on that area. The glacier area within each grid cell is removed from the land area simulated by WBM; all water accumulation and runoff from that land area is taken from the glacier input dataset. WBM assumes that this land area, which is typically a fraction of a grid cell, sits at the highest elevation within the grid. To avoid double-counting precipitation inputs onto this land area (which is accounted for by the glacier input dataset), WBM reduces grid cell precipitation linearly by the fraction of the grid cell covered by glacier area. Each glacier has a single designated outlet location even in the case that the full glacier covers multiple grid cells, and it is also assumed that runoff from the glacier area all flows directly into the outlet grid cell's river system. These methods are first described in (Mishra et al., 2020), and were developed to make use of rasterized output from the Python Glacier Evolution Model (PyGEM; (Rounce, Khurana, et al., 2020)). PyGEM's standard output format is not gridded; rather, post-processed PyGEM output is required as input for WBM (Prusevich, et al., 2021).

265

270

### 2.2.2 Groundwater

*Shallow groundwater storage pool:* As noted above, when water enters a grid cell in excess of the volume that can be stored in soils, the canopy, and lost via evapotranspiration, then runoff and recharge both occur. The portion of that excess water that becomes recharge is defined by the recharge fraction parameter, with a default value of 0.5. Alternative non-default input values can be a constant applied to the whole simulation domain, or a gridded layer to reflect its spatial variability. The recharge water enters a below-soil storage pool called the shallow groundwater storage pool. This shallow groundwater pool generates baseflow (i.e., subsurface runoff) by leaking water to the river system stream reaches in the same grid cell where recharge occurred at a rate defined by a hydrodynamic groundwater constant (default 0.025 1/d), described in Wisser et al. (2010a) and Grogan (2016).

275

280

*Unsustainable groundwater:* Following the GHM methods of (Hanasaki et al., 2008a; Wada et al., 2012), WBM additionally represents an unsustainable groundwater source. WBM's implementation of unsustainable groundwater was first described in Wisser et al. (2010a), and again in Grogan et al. (2015; 2017), Liu et al. (2017), and Zaveri et al. (2016). The unsustainable groundwater source is not defined as a stock, and so no state variable is associated with it. When the demand for water extractions (see Section 2.2.5 below) exceeds the water supply available from surface water and shallow groundwater, WBM has the option to allow the residual, or a parameter-defined fraction of the residual, to be supplied from an unlimited unsustainable groundwater source. This effectively defines unsustainable groundwater use – known alternatively as groundwater mining or the use of fossil groundwater – as any groundwater extraction in excess of the long-term recharge rates applied to the shallow groundwater pool and represents an additional source of water entering the

285

290



simulated hydrologic system. Prior work (e.g. (Gleeson et al., 2012; Grogan et al., 2015; Grogan et al., 2017; Wada et al., 2012; Zaveri et al., 2016) has shown that assuming that this unsustainable water source is available is reasonable at a macro-scale, and allows GHMs to evaluate aquifer mining at large scales and compare to groundwater-based mass change  
295 observations from the GRACE satellite (Sutanudjaja et al., 2018).

### 2.2.3 River discharge

WBM has a horizontal water transport model that represents the flow of rivers in one dimension. The foundation of this model is the digital river network, which defines exactly one flow direction for each grid cell. As grid cells connect into  
300 networks, these form the representation of river systems. Note that every grid cell has a flow direction, regardless of whether enough water accumulates to actually flow through the grid cell or not (e.g., an arid region with no or low precipitation would have no flow, but would have a defined network of flow directions, as described by STN-30p network (Vörösmarty et al., 2000b)). The model offers two options for how to calculate river flow velocity: 1) a Muskingum-Cunge solution of the Saint-Venant flow equations (Maidment, 1993), and 2) a linear reservoir routing solution. We find that the Saint-Venant  
305 flow equations are appropriate only for simulations of relatively coarse grid cell resolution – half-degree by half-degree or larger – where much of the river’s volume remains within the grid cell over a 24-hour time period. For the finer resolution simulations – 5-minute grid cell size and smaller – that are now common amongst many GHMs, the linear reservoir routing method is more appropriate. The Muskingum-Cunge solution is fully documented in Wisser et al. (2010a) and Grogan (2016), and the linear reservoir routing method follows common formulations (Dingman, 2002, p. 429). Both are described  
310 again in the model documentation that accompanies the code on GitHub (<https://github.com/wsag/WBM/tree/main/documentation>).

*Hydraulic geometry:* WBM incorporates both downstream and at-a-station stream geometry relationship assumptions to calculate river width, depth, and velocity from discharge. WBM assumes that each grid cell has a single representative  
315 stream reach and calculates a rolling average of annual mean discharge for each reach in a simulation over the previous five-years of a simulation. The long-term mean discharge,  $\bar{Q}$ , [m<sup>3</sup>/s] is then used to estimate the long-term mean depth,  $\bar{z}$  [m], width,  $\bar{y}$  [m], and velocity,  $\bar{u}$  [m/s], using down-stream hydraulic geometry relations and scalers from (Park, 1977):

$$\bar{z} = \eta \bar{Q}^{\nu} \quad (19)$$

$$\bar{y} = \tau \bar{Q}^{\phi} \quad (20)$$

$$320 \quad \bar{u} = \delta \bar{Q}^{\epsilon} \quad (21)$$

where  $\eta$ ,  $\nu$ ,  $\tau$ ,  $\phi$ ,  $\delta$  and  $\epsilon$  are user defined variables, with optional default values listed in Table 2.

Instantaneous estimates of the three variables ( $z$  [m],  $y$  [m], and  $u$  [m/s] for depth, width and velocity, respectively) are given as functions of instantaneous  $Q$  [m<sup>3</sup>/s] and mean discharge  $\bar{Q}$  [m<sup>3</sup>/s], scaled by appropriate at-a-station hydraulic geometry exponents (Dingman, 2009):



325 
$$z = \bar{z} \left( \frac{Q}{\bar{Q}} \right)^f \quad (22)$$

$$y = \bar{y} \left( \frac{Q}{\bar{Q}} \right)^b \quad (23)$$

$$u = \bar{u} \left( \frac{Q}{\bar{Q}} \right)^m \quad (24)$$

In the above equations, parameters  $f$ ,  $b$  and  $m$  are all user defined variables, with optional default values from (Leopold & Maddock, 1953), listed in Table 2.

330

**Table 2.** Default hydraulic geometry parameter values.

Parameter	Default Value
$\eta$	0.25
$\nu$	0.40
$\tau$	8.00
$\phi$	0.58
$\delta$	2.18
$\epsilon$	0.02
$f$	0.40
$b$	0.10
$m$	0.50

#### 2.2.4 Hydro-infrastructure

335 *Dams and reservoirs:* Large dams and reservoirs alter river flows and provide water supplies to surrounding areas. Provided a database containing the required information, WBM simulates the impact of reservoir operations on river flow, and it uses the water stored in reservoirs as supply for water extractions and consumptive uses (see Section 2.2.5 below). The input dam database must have the following information to be of use to WBM: the year of dam construction, the reservoir area and capacity, the upstream catchment area, the main purpose, and the location. The database may optionally include information on the year a dam was removed, if applicable. Dam databases with this information include the Global Reservoir and Dam Database (GRanD; (Lehner et al., 2011)), and the Hydrologically Consistent Dams Database (HydroConDams; (Zuidema & Morrison, 2020)).

345 WBM employs a general reservoir water release rule, with parameter modifications for dams of different purposes such as irrigation supply or flood control. A general water release rule is designed to maintain outflows approximately equal to average annual inflows, but to release less water when reservoir levels are low and more water when reservoir levels are high. Water levels considered “high” or “low” are based on the purpose of the dam and can be parameterized for specific dams or set of dams. Dams on irrigation reservoirs are additionally parameterized with a time series of downstream irrigation water requirements, ensuring that water is released downstream from the dam during the time of greatest water extraction demand. In reality, many irrigation reservoirs are connected to downstream irrigated areas by canal systems that flow

350 directly from the reservoir and do not rely on dam operations. WBM does not represent these canal systems, and so uses dam



water releases to account for this canal-enabled downstream flow of water. Full reservoir release methods, along with parameter values assigned to different dam types, are documented in (Rougé et al., 2021). Alternatively, discharge out of individual dams can be input directly to WBM, thereby making calculated reservoir storage a function of observed reservoir output (Zuidema et al. 2020); this ensures releases match historical records in cases where WBM's default functions vary too far from observed reservoir operations.

*Small irrigation reservoirs:* Rainwater harvesting for irrigation water supply is represented in WBM's small irrigation reservoir module. These small reservoirs do not dam rivers as larger reservoirs do, and so do not alter river flow. Rather, they collect rainwater and surface runoff, storing it on the land surface and preventing it from reaching the rivers system. Note, these are not run-of-river reservoirs, but structures on the land surface. We do not know of any global or even regional dataset that describes the location and capacity of these small irrigation reservoirs. WBM's small irrigation reservoir methods were developed and first described in (Wisser et al., 2010b), where a range of capacities were simulated to provide a sensitivity analysis and quantify the potential importance of these highly localized water supply systems.

*Inter-basin transfers:* Inter-basins transfers are large canals, tunnels, or pipelines that move water across river basin boundaries. These large projects alter flows in both the sending and receiving river systems and can be used to supply water for consumptive uses. WBM simulates how inter-basin transfers alter the flows in both the sending and receiving rivers, though it does not explicitly represent the routing of water discharge through the canal system. WBM's inter-basin transfer methods were first developed and described in (Zaveri et al., 2016) and described again in (Liu et al., 2017). Five parameters are used to simulate the water transfer: the water sending point latitude and longitude, the water recipient latitude and longitude, a minimum allowed sending river flow, a maximum allowed canal intake flow, and a water release rule for flow volumes between the minimum and maximum. A database of India's inter-basin transfers was used by WBM in (Zaveri et al., 2016) and is included as supplemental information to that publication.

### 2.2.5 Water extraction and consumptive water use

Water extractions from rivers, reservoirs, and groundwater are an important part of simulating water supply and changes in human-hydrologic interactions. WBM first implemented water extractions for irrigated agriculture (Wisser et al., 2008; Wisser et al., 2010a), which globally is known to account for ~70% of all freshwater extractions (Rosegrant & Cai, 2002). Modules for water supply for livestock, domestic, and industrial use, which are less consumptive than irrigation water and account for a smaller proportion of total global extractions, were added to WBM in (Liu et al., 2017). When water is removed from a storage (e.g., reservoirs or the shallow groundwater pool), the storage value of that stock is updated within the daily time step.



385 Water withdrawals are taken from different water stocks and fluxes based on a given priority order of both water users and  
water sources; this rule set has a number of user input options and parameters making it highly flexible and customizable.  
The default priority order for withdrawal by water users within a grid cell is: (1) domestic, (2) industrial, (3) livestock, and  
(4) irrigation. In turn, the withdrawals from each user group come from water storage and flux pools in the following order  
until the requested withdrawal water volume is met:

- 1) Small irrigation reservoirs (available to livestock and irrigation water use only);
- 390 2) Shallow groundwater. When shallow groundwater is extracted for domestic, industrial, and livestock use, all the water  
in the shallow groundwater pool can be extracted, up to the volume requested by the sector. When this source is  
extracted for irrigation, an optional parameter,  $r_{sg}$  [-], defines the target ratio of groundwater-to-total withdrawals for  
irrigation water extractions. This parameter can be a constant or a spatially variable grid. If  $r_{sg}$  is not defined, then all  
available shallow groundwater is extracted for use (up to the water demand) in this step. In the case that  $r_{sg}$  is defined,  
395 then this first groundwater withdrawal step takes water from shallow groundwater,  $SG$ , up to the volume defined by the  
product of  $r_{sg}$  and irrigation water demand, even if there is more shallow groundwater available and the irrigation water  
demand,  $D$  [mm], is greater than the defined water amount, such that shallow groundwater withdrawal,  $W_{sg}$ , is at this  
step is:

$$W_{sg} = \min(r_{sg}D, SG) \quad (25)$$

- 400 3) Surface water in a river or reservoir within the same grid cell. Stream water available for extraction is estimated as 80%  
of water retained in river and reservoir storage following routing during the previous time-step  $W^{k-1}$ , plus the volume,  
 $V_{stream}$ , represented by flow through the reach during the previous time-step:

$$V_{stream} = Q^{k-1}dt + W^{k-1} \quad (26)$$

- 405 4) Shallow groundwater – second extraction for irrigation only. If the parameter  $r_{sg}$  is defined in a way that limited shallow  
groundwater extraction for irrigation to less than the available shallow groundwater volume in Step 2, and there is still  
residual water demand, then at Step 4 water volumes up to the remainder of the shallow groundwater storage volume  
can be extracted. By combining Steps 2 and 4, the target irrigation groundwater-to-total withdrawal ratio is achieved  
only in the case that the sum of surface and shallow groundwater volumes is sufficient to meet this ratio; Step 4 ensures  
that fulfilling water withdrawal demands using sustainable resources within the grid cell takes priority over achieving  
410 the target ratio. This step does not apply to livestock, domestic, or industrial water extractions, as no ratio parameter is  
applied to those water uses.
- 5) Surface water in a river or reservoir outside the given grid cell that has the largest storage + discharge volume within a  
set of parameter-defined radii. A different parameter can be set for irrigation water use than for other uses, representing  
the differences in irrigation and municipal water supply infrastructure. The default radius value is 100 km for all water  
415 uses; the user can define a set of alternative constant scalars or gridded layers of values.



6) Unsustainable groundwater (UGW). Water available for extraction from this pool may be limited by the UGW allowance ratio, if defined. Because this source of water has no stock value, the allowance ratio applies a scaler of  $\leq 1$  to the water withdrawal demand. This scaler is independent of  $r_{sg}$ , and if not defined, this pool is unlimited.

420 *Irrigation*: Given inputs of irrigated land area and associated crop-specific parameters, WBM calculates the agronomic water requirements for optimal crop growth over its three growing seasons: (1) planting and development, (2) growth, and (3) harvesting. In WBM, crops extract water from the soil moisture pool each day of the crop's growing season. Given sufficient water in the soil moisture pool, the amount of water used by each crop is the crop's potential evapotranspiration. When soil moisture levels drop below a crop-specific threshold, the difference between the soil moisture level and field capacity is defined as the irrigation water requirement. This method of crop irrigation water requirements follows FAO guidance (Allen et al., 1998), as is typical of GHMs. WBM's crop irrigation water requirement methods have been described in: Grogan et al. (2015, 2017), Liu et al. (2017), Wisser et al. (2010a), Zaveri et al. (2016) and Zuidema et al. (2020).

430 Alternatively, WBM has the option to calculate a daily crop gross irrigation water requirement instead of using the crop-specific soil moisture threshold to trigger water extractions. When using this option, WBM estimates gross crop irrigation water requirements each day, equal to the difference between soil moisture content and field capacity and modified by either the classical irrigation efficiency parameter or the irrigation technology-derived classical efficiency for the day (described below). Irrigation water is then extracted from water sources each day, and stored in an irrigation water storage pool that doesn't interact with other fluxes within the model until the day when the crop-specific soil moisture threshold is reached. 435 When this threshold is reached, water is moved from the irrigation water storage pool to the soil moisture. This option extracts relatively small amounts of water from water stocks each day, instead of larger amounts of water on the day that the soil moisture threshold is reached.

440 The amount of water required by a crop to achieve  $AET = PET$  is less than the amount of water that must be extracted from a water source due to inefficiencies in irrigation water extraction, transportation, and application. WBM has two options for calculating the gross irrigation water extraction required as a function of net irrigation water required by the crop: (1) the irrigation efficiency method, and (2) the irrigation technology method.

445 The irrigation efficiency method is standard for GHMs and described in Grogan et al. (2015, 2017), Liu et al. (2017), Wisser et al. (2010a), and Zaveri et al. (2016). In this method, classical irrigation efficiency is an input to WBM and directly modifies the net irrigation water requirement by a spatially varying constant. Classical irrigation efficiency is defined as the ratio between net irrigation water required and gross water extractions. Net irrigation water requirements include water transpired by the crops, and associated soil evaporation that is unavoidable. As described in Grogan (2016) and Wisser et al. (2010a), net irrigation water requirements for rice paddies also include an additional water volume, representing the water



450 needed to enable flooding at the start of the growing season and maintenance of the flood paddy water level throughout the  
season to compensate for percolation. The volume of water added to initially flood the rice paddies is an input parameter  
with a default value of 50 mm of depth applied over all irrigated paddy rice areas. The daily additional water application rate  
used to maintain the paddy depth is based on the rate of water percolation through the underlying soils. This is also an input  
dataset, with methods for calculating percolation rates from soil property data described in Wisser et al. (2010a). Both the  
455 initial paddy flood water and the daily maintenance water are included in irrigated rice's net irrigation water volume, and the  
irrigation efficiency parameter is applied to these volumes in the same way it is applied to other net irrigation water  
requirements.

The irrigation technology method in WBM is first described in Zuidema et al. (2020), and represents non-consumptive  
460 irrigation water losses as a function of irrigation technology-specific parameters and open water evaporation rates (which can  
be input or calculated as a function of weather inputs). In this second method, inputs on the spatial distribution of different  
irrigation water conveyance and application technologies (Jägermeyr et al., 2015, 2016) is required, and the inefficient water  
losses that occur over space and time are calculated within WBM as a function of irrigation technology type and weather  
variables. Classical irrigation efficiency is therefore calculated and provided as a time- and space-varying model output.

465 *Blue water and green water use for irrigation:* Falkenmark and Rockström (2006) introduced the concept of “blue water”  
and “green water” into the GHM literature to distinguish between direct precipitation and irrigation water sources in crop  
ET. Blue water is defined as liquid water that can be extracted from aquifers, surface water reservoirs (lakes and dams), and  
river systems, and Green water is defined as soil moisture water originating from direct precipitation (including snowmelt)  
470 (Falkenmark and Rockström, 2006). WBM can estimate the flux of blue and green water via evapotranspiration by irrigated  
crops. Note that all evapotranspiration from rainfed crops is by definition green water. All water that becomes irrigated crop  
evapotranspiration must first enter the soil moisture pool. Water enters the soil moisture pool by either (1) direct  
precipitation or snow melt, which is Green Water, or (2) irrigation from surface or groundwater, which is blue water. We  
assume that water in the soil moisture pool is well mixed on a daily time step. Therefore the evapotranspiration out of that  
475 pool has the same proportions of blue and green water as the soil moisture pool itself. Optional model output variables  
include the grid cell average soil moisture that is made up of blue and green water [mm], grid cell total evapotranspiration of  
blue and green water from the soil storage pool [mm/day], crop-area specific soil moisture values of blue and green water  
[mm] (e.g., blue water stored in soils under a specified input crop type), and crop-specific evapotranspiration of blue and  
green water [mm/day].

480 *Livestock:* Livestock require water for drinking and for service water, which includes washing and cooling. WBM uses the  
methods and default parameter values (Table 3) provided by Steinfeld et al. (2006) to calculate livestock water use by animal  
type. Daily livestock water,  $L_v$  [m<sup>3</sup>/d], for each livestock type is calculated each day as:





$$L_w = (I_l + s_l T + B_l) D_l \quad (27)$$

485 where  $I_l$  [ $\text{m}^3/\text{head}/\text{day}$ ] is the minimum water demand for livestock type  $l$ ,  $s_l$  [ $\text{m}^3/\text{head}/^\circ\text{C}/\text{day}$ ] is the temperature induced  
 consumption requirement for livestock type  $l$  [-],  $T$  is the daily mean temperature, with a minimum value of 0 [ $^\circ\text{C}$ ];  $B_l$   
 [ $\text{m}^3/\text{head}/\text{day}$ ] is the daily service water volume required per animal, and  $D_l$  is the density of livestock type  $l$  in the grid cell  
 [animal head/grid cell]. Additionally, an animal population growth rate can be applied to each livestock head density  
 490 category to represent increases in population over a given single-year value of animal head density data (the year of  $D_l$ , input  
 reference livestock density). This is useful as limited global livestock density data is available. Livestock is assumed to  
 consume 5% of its water extractions, with the remaining 95% returning to the system via runoff; the ratio of consumption to  
 return flows can be modified by user-defined input parameters.

**Table 3.** Default livestock parameters for the livestock water use module.

Livestock	Slope, $s_l$	Intercept, $I_l$	ServiceWater, $B_l$	Population Growth Rate
buffalo	0.345	16.542	5	0.001863
cattle	0.345	16.542	5	0.001863
goats	0.215	4.352	5	0.003731
pigs	1.4575	-6.14	25	0.000309
poultry	0.019	0.1823	0.09	0.13397
sheep	0.57	-0.35	5	0.003

495

*Domestic and industrial:* Households and industry extract water for a range of purposes, and at rates that have great spatial  
 variability. WBM represents these extractions based entirely on an input per capita water extraction rate and a population  
 density map, such that domestic water use,  $U_d$  [ $\text{m}^3/\text{grid cell}/\text{day}$ ], is:

$$500 \quad U_d = u_{dom} A D_{pop} \quad (28)$$

And industrial water use,  $U_i$  [ $\text{m}^3/\text{grid cell}/\text{day}$ ] is:

$$U_i = u_{ind} A D_{pop} \quad (29)$$

Where  $A$  [ $\text{km}^2$ ] is the area of the grid cell,  $u_{dom}$  [ $\text{m}^3/\text{person}/\text{day}$ ] is the per capita domestic water withdrawal,  $u_{ind}$   
 [ $\text{m}^3/\text{person}/\text{day}$ ] is the per capita industrial water use, and  $D_{pop}$  [ $\text{persons}/\text{km}^2$ ] is the population density. Domestic and  
 505 industrial water use each have unique return fraction coefficients, which default to uniform values of 84% and 89%  
 respectively.

### 2.2.6 In-stream nitrogen and water temperature

*Nitrate-nitrogen concentration:* WBM estimates in-stream and in-reservoir nitrate-nitrogen ( $\text{N-NO}_3$ ), dissolved organic  
 510 nitrogen (DIN), and/or total nitrogen (TN) concentration. In-stream  $\text{N-NO}_3$  concentrations are a function of point source  
 nitrate inputs from wastewater treatment plants, non-point source nitrate inputs from the land surface, and in-stream



denitrification. Wastewater treatment plant contributions to in-stream nitrate are calculated using data on served population and waste treatment type, as described in (Samal et al., 2017). Nitrate inputs from land are estimated as a function of simulated grid cell runoff and the estimated nitrate concentration in runoff from different land use types. Estimation of land use-specific runoff nitrate concentrations are described in Wollheim et al. (2008a). The suite of parameters describing nitrate concentration in runoff from different land use types may require region-specific calibration, but the model default values are found to be adequate for moderately developed landscapes with modest agricultural cover (Samal et al., 2017; Simon, 2018; Stewart et al., 2011a). In-stream (Stewart et al., 2011a) and in-reservoir (Simon, 2018) denitrification are calculated using temperature-corrected denitrification along the benthic surface assuming efficiency loss kinetics, following (Mulholland et al., 2008; Wollheim et al., 2014).

*Water temperature:* River temperature is calculated following (Stewart et al., 2013). Temperature is first calculated on the landscape, mixing air temperatures depending on the timing of shallow groundwater recharge. River temperature equilibration is then calculated through a combined empirical and deterministic re-equilibration procedure given by (Dingman, 1972). The reequilibration is a function of channel hydraulics, air temperature, solar radiation, humidity, and wind speed.

### 2.2.7 Water source tracking

WBM tracks water from each source (water inputs to each individual grid cell) through all flows and stocks within the model. Stocks within each grid cell include soil moisture, small reservoir storage, shallow groundwater storage, surface retention and irrigation storage pools, rice paddy flood waters, river storage, and large reservoirs. Flows are infiltration into soils, surface runoff, recharge to shallow groundwater, baseflow, river discharge, water discharge from reservoirs, evaporation, evapotranspiration, inter-basin transfers, water extracted for human water use, and return flows from human water use. These stocks and flows are depicted in Figure 2. WBM's tracking functionality retains information about the generative mechanism (i.e., the water source) as water flows across the landscape through the river network. This includes through processes such as extraction for human use, and subsequent redistribution according to hydrologic flow-paths.

The same tracking algorithm applies to all water source components. For any water component  $c$  in water storage stock  $S$  at timestep  $k$  in a given grid cell:

$$S_c^k = \frac{(S_c^{k-1} \cdot S^{k-1}) + \sum_i (I_{c,i} I_i) - \sum_j (S_c^k O_j)}{S^k} \quad (30)$$

where  $S_c^k$  is the fraction of stock  $S$  composed of component  $c$  at time  $k$ .  $S^k$  is the total volume of stock  $S$  at time  $k$ .  $I_i$  are inflows to and  $O_j$  are outflows from stock  $S$ , with  $I_{c,i}$  the fractions of the  $i$ th flow composed of component  $c$  all at timestep  $k$ . Component stocks ( $S_c^k$ ) are updated throughout the timestep such that the solution is split into multiple operators as the various fluxes impact each stock.



545 WBM performs three types of component tracking: primary source component tracking (Fig. 2) representing the initial input  
of water into the water balance equations, return flow component tracking representing water that has been reintroduced to  
the hydrologic cycle following human extraction, and runoff from labeled land attributes (Table 4). Primary source  
components were first described in Grogan et al. (2017), where only the unsustainable groundwater component was  
analyzed. Return flow components were first described in Zuidema et al. (2020); land cover mask components have not yet  
550 been described in the literature.

All stocks and flows are considered well-mixed, so that the flows out of a stock have the same fractional water source  
components as the stock itself. All stocks are initialized with  $S_c = 1$  for one of the set of components that are tracked. For  
example, in primary source component tracking, all stocks are initialized as 100% rain water; as the model goes through a  
spin up stage, water from the other components are added to these stocks. At the beginning of a simulation, large reservoirs  
555 are initialized at 80% of their full capacity, the soil moisture storage pool is initialized at 50% of capacity, and all other  
stocks begin at 0% capacity. We recommend a minimum spinup time of 10 years to allow all stocks to reach equilibrium  
storage, and importantly for many stocks to accumulate the different tracked water components. WBM operates at a daily  
time-step, and for some stocks (e.g. river discharge) our well-mixed assumption is appropriate; however, other stocks are  
typically not well-mixed at the daily time-scale (e.g. soil, reservoirs (Håkanson, 2005), or groundwater (Hrachowitz et al.,  
560 2013)). Therefore, we consider these fluxes with caution at short time-scales (days to years), but find them informative when  
averaged over long-periods (years to decades).

Return flow tracking has an additional option for re-setting the stock component values after spinup has completed. At  
the end of spinup (prior to the simulation period), stocks can be reset to 100% relict water. This option allows the user  
565 to interpret changes to stock components that occur only within the simulation period, removing assumptions about  
starting compositions. This option is one way to explicitly track the fate of components that enter the simulation at the  
onset of the representative simulation period (Zuidema et al., 2020).

Note that the land surface label tracking can track multiple land labels at once that can include sets of political  
570 boundaries, land-cover types, soil types, biogeographic or climate zones, or other identifiers such as the grid cell  
Strahler stream order or distance of a grid cell from the river mouth. These land labels can occupy entire grid cells, or  
be provided as a set of grid cell fractional coverage (i.e., a percentage of each grid cell is covered by each label type).  
WBM will track each identified land label with a unique numerical ID input via a raster-based mask of unique values.

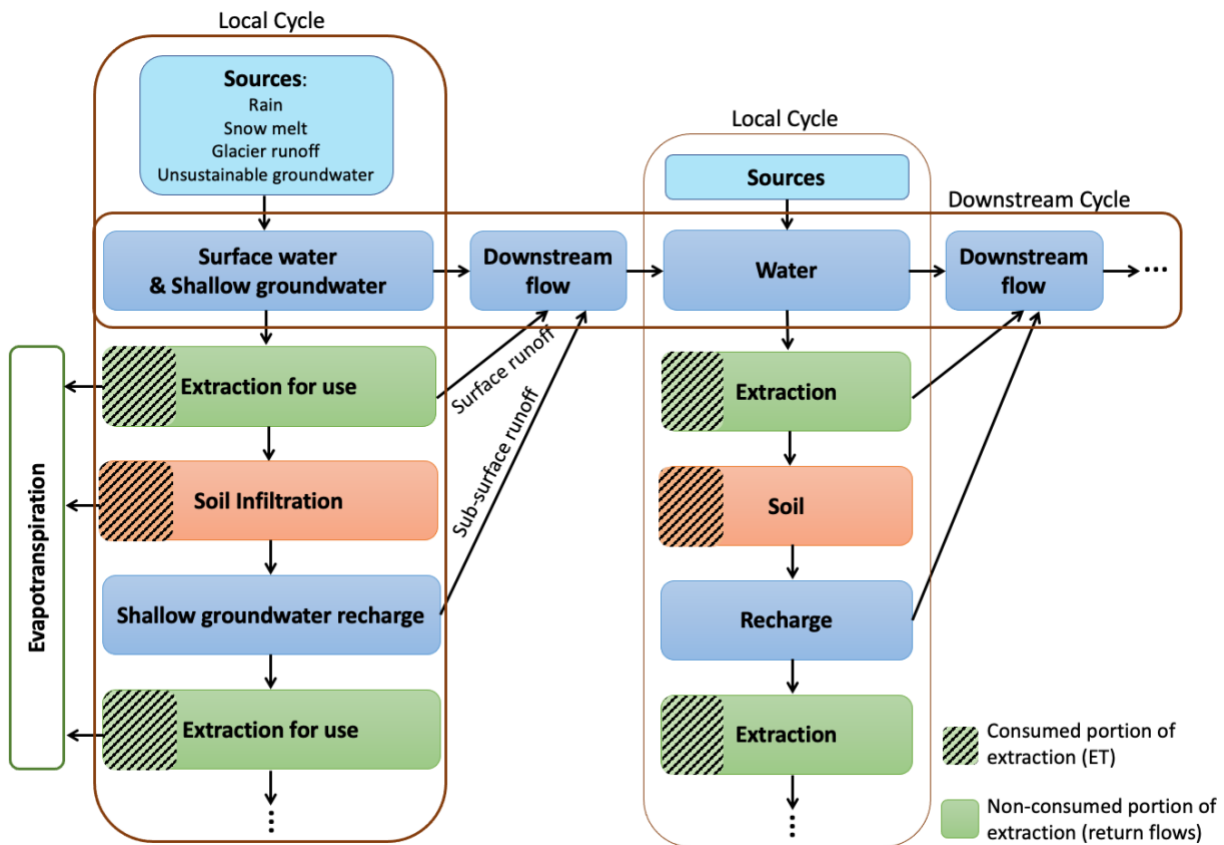
575



**Table 4:** Tracking component categories, and the identification of the water source components tracked

Tracking group	Water components tracked
Primary Source Components	Rain* Snow Glacier runoff Unsustainable Groundwater
Return Flow	Pristine (no return) Domestic/Livestock/Industrial returns Irrigation returns Relict*
Land surface labels	ID_1, ID_2, ..., ID_N

\*This component comprises 100% of reservoir and soil moisture stocks prior to spinup



580

**Figure 2:** Primary source component tracking schematic. All surface and shallow groundwater is composed of the four primary sources: rain, snow melt, glacier runoff, and unsustainable groundwater. When surface and/or shallow groundwater



585 is extracted for use, this initiates both a local cycle and a downstream cycle of water use and re-use. In the example shown  
here, water is extracted and applied to soils (irrigation). A portion of the extracted water and a portion of the soil water  
becomes evapotranspiration (the consumed portion, shown with hashes). Some of the water applied to soils percolates to the  
shallow groundwater pool. Water from the shallow groundwater pool can be extracted again, continuing the local water re-  
use cycle. Water extracted for use, and water from the shallow groundwater pool, generate runoff that moves downstream.  
This initiates a downstream cycle in which this water can be re-extracted for use from the surface water system. Downstream  
cycles intersect with local cycles, as water from the four primary sources are input in every locality. Figure modified from  
590 Grogan et al. (2017).

### 3 Model evaluation

River discharge is the observational data against which most GHMs validate, in part due to the abundance of high quality  
global river discharge data and in part due to the fact that river flow is an integrative result of all the land surface fluxes  
595 simulated by GHMs. Here we first summarize published validation of WBM output in recent relevant papers (section 3.1).  
We make note of where these validations make use of prior code branches (e.g., the C++ version of WBM, or FRAMES) or  
are regionally-specific. Then we present a validation of global river discharge simulated by the open source WBM version  
described here (section 3.2). We also evaluate the model's estimation of water extraction for irrigation against the only  
global dataset available for this metric.

600

#### 3.1 Published WBM validation

This section reviews the literature of WBM publications that include validation of model components that are included in the  
WBM open source model. These papers report a variety of different evaluation metrics, which we summarize here.

605 *Global river discharge:* The Perl/PDL version of WBM (which is described here) was most recently validated against global  
discharge from the Global Runoff Data Centre reference dataset (GRDC,  
[https://www.bafg.de/GRDC/EN/04\\_spcldtbss/43\\_GRfN/refDataset\\_node.html](https://www.bafg.de/GRDC/EN/04_spcldtbss/43_GRfN/refDataset_node.html)) in (Grogan, 2016). Grogan (2016) reports  
that a linear regression of modeled versus observed average annual river discharge for the years 1980 – 2009 typically shows  
strong agreement ( $r^2$  values between 0.74 and 0.87), but that this agreement varies with the choice of input climate data set  
610 (Fig. 3). The ERA-Interim (Dee et al., 2011) and NCEP (Saha et al., 2014) climate inputs were found to provide the best  
global discharge simulations, with over 40% of all GRDC stations achieving a Nash-Sutcliffe Efficiency (NSE; Nash and  
Sutcliffe, 1970) of  $> 0$ . There is also spatial variation in model performance; as can be seen in Grogan (2016), WBM river  
discharge matches observations best in temperate and tropical regions, but performs poorly in arid climates. Spatial variation  
in validation is also in part due to the choice of climate inputs. For example, the cluster of outliers in Fig. 3a are all from the  
615 same river basin, the Congo. Overall WBM simulations from Grogan (2016) are biased low compared to observations, which  
can be seen by comparing the 1:1 lines with the trendlines in Fig. 3. These results are consistent with global river discharge  
validation of the C++ version of WBM (also called WBMplus) in Wisser et al. (2010a), who report an average Model Bias  
Error (MBE) of runoff of  $-1.2 \text{ mm month}^{-1}$  from 1901 – 2002. Fekete et al. (2002) also compared WBM (C++ version)



620 global river discharge to GRDC data, and reports a positive mean bias in runoff of  $7.9 \text{ mm yr}^{-1}$ . All three published global river discharge validations show that simulated discharge performs better in larger catchments than in smaller ones.

625 *Regional river discharge:* The global simulations described above used a grid cell resolution of 0.5 degrees. WBM can be used for sub-continental scale, or regional, studies; in this case, a finer spatial resolution must be used, and model parameters calibrated to better fit local conditions, and regional river discharge data is used for validation. Grogan (2016) and Zaveri et al. (2016) validated WBM against river discharge data in India, using discharge and runoff data from the India Water Resources Information System (India-WRIS) and FAO AQUASTAT (Frenken, 2012), respectively. They report that the Nash-Sutcliffe Efficiency (NSE; Nash and Sutcliffe, 1970), a typical hydrologic validation metric, is  $> 0$  (i.e., better than predicting the mean of historical observations) for 15 of the 20 IWRIS sites, and average annual runoff from WBM compares well with AQUASTAT reports for the 8 largest river basins in India. These continental-scale simulations of India 630 used the same 0.5 degree spatial resolution as the global simulations. A finer,  $\sim 100 \text{ km}^2$  (6 arc-minute) grid cell resolution simulation of northeastern North America had NSE values  $> 0$  at 82% of the 791 USGS gage stations used for comparison in Grogan et al. (2020). A very fine resolution, 1 km grid cell scale simulation of the Trishuli Basin in Nepal is evaluated in Mishra et al. (2020), where overall agreement with reported monthly mean river discharge is shown (NSE  $> 0.7$ ), though seasonal variation shows that WBM underestimates summer high flows in some years, and in other years over-estimates high 635 flows over a period of 11 years. A similarly fine-resolution simulation ( $\sim 1 \text{ km}$ ) of the Upper Snake River Basin of Idaho, U.S., is evaluated in Zuidema et al. (2020); seasonal discharge in headwaters compares well (NSE = 0.9) with USGS gage data, though WBM demonstrates a positive bias (discharge values are too high) and large variation in seasonal discharge in the basin's small tributaries. All fine resolution WBM simulations described here used non-default parameter sets that were calibrated to regional data, unlike the global runs described above. Even with regional calibrations the simulations result in 640 similar outcomes as the global analyses: WBM river discharge typically compares well to observations, though better in larger than smaller river basins, and better when aggregated to a monthly time step rather than daily. Default parameters provide good performance at large (continental to global) scales, but calibration is required for local to regional studies to account for local deviations of parameters from the global means. Additionally, simulated river discharge disagrees with observations immediately downstream of dams that either aren't represented in the input dam database, or that are operated 645 with decision rules not captured by WBM's reservoir operation algorithms, as described in Rougé et al. (2021).

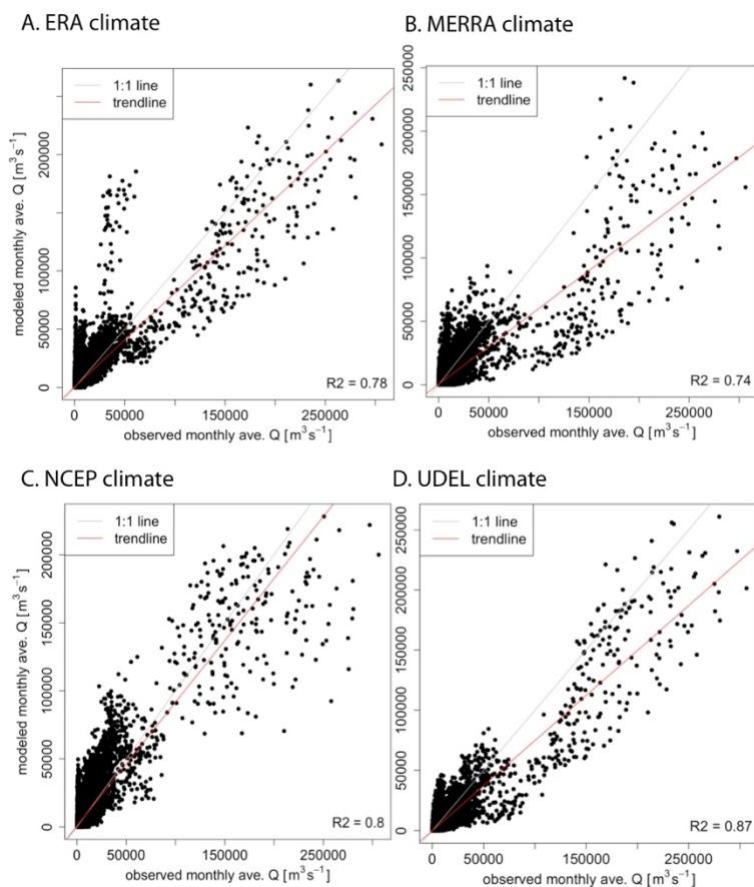


**Figure 3.** WBM modeled monthly average river discharge is plotted against observed monthly average river discharge from the Global Runoff Data Centre (GRDC). The four panels show WBM simulations that use four different climate input datasets for the years 1980 – 2009: (a) ERA-Interim (Dee et al., 2011); (b) MERRA (Rienecker et al., 2011); (c) NCEP (Saha et al., 2014); and (d) UDEL (Willmott and Matsuura, 2001). Figure reproduced from Grogan (2016).  
650

*Irrigation water extractions:* WBM is often used for agricultural applications, and so has been well validated against FAO country-level reported irrigation water extraction data globally in Grogan (2016), Grogan et al. (2017), Wisser et al. (2008), Wisser et al. (2010a) (Fig. 4), and regionally in Zaveri et al. (2016) and Zuidema et al. (2020). Notably, Wisser et al. (2008)  
655 quantifies the high uncertainty in irrigation water withdrawals as a function of input climate and crop map data. Globally, WBM-simulated average total irrigation water extraction for the years 1963 – 2002 varies from  $2,200 \text{ km}^3 \text{ year}^{-1}$  to  $3,800 \text{ km}^3 \text{ year}^{-1}$  in Wisser et al. (2008), with the large difference in values due entirely to the choice of climate input and crop map. While the validation data used in all the WBM publications is fully independent of model input data, it should be noted that most irrigation water extraction data are reported statistics, not direct observations.

660

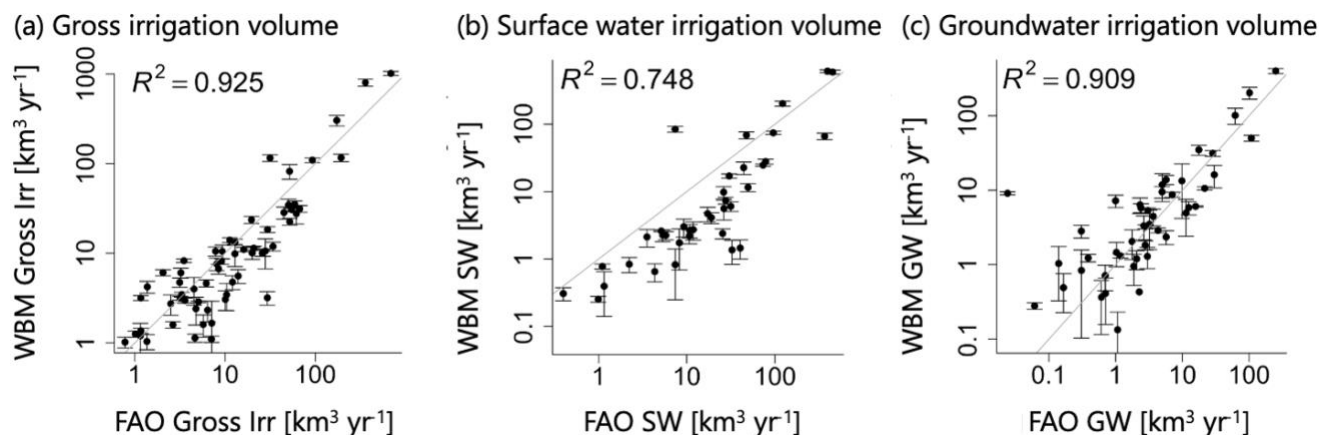


**Figure 4.** WBM modeled annual irrigation water withdrawals compare well to FAO AQUASTAT (FAO, 2016) country-level reported (A) total irrigation, (B) surface water use, and (C) groundwater use. Note that both the x and y axes are on a log scale. Figure reproduced from Grogan et al. 2017.

665

*Additional validation metrics:* In addition to river discharge and irrigation water extractions, regional studies have validated against metrics that are relevant to their application. For example, Zaveri et al. (2016) qualitatively validated WBM's change in groundwater levels in the Indian state of Punjab using well level data; Grogan et al. (2020) validated simulated snow water equivalent across northeastern North America, and Zuidema et al. (2020) evaluated WBM's snowmelt onset timing.

670

*Validation of FrAMES:* The FrAMES model (Wollheim et al., 2008a,b; Stewart et al., 2013) functions for river temperature and in-stream nitrogen concentrations have been incorporated into the open source version of WBM described here. While there has yet to be a published validation of the open source WBM implementation of these functions, the FrAMES model nitrogen functionality is evaluated globally in Wollheim et al. (2008a) and regionally in Samal et al. (2017) and Stewart et al. (2011b). River temperature simulations are validated across northeastern North America in (Stewart et al., 2013). FrAMES also has an in-stream chloride module; while WBM does not yet have this module implemented, chloride is an informative metric for evaluating river discharge as this solute is a conservative tracer. We report FrAMES chloride validation findings here to show how well discharge matches observations, as the river discharge functions in WBM and FrAMES are the same. In Zuidema et al. (2018), simulations of river discharge, temperature, and chloride in the Merrimack and Piscataqua River watersheds of New England, U.S., were assessed using approximate Bayesian computation (Sadegh & Vrugt, 2013), which provides information on the best regional parameterization for the model. The best parameter estimates resulted in simulated flow-duration curves with an NSE of 0.93 compared to USGS gage data. Further, Zuidema et al. (2018) found that default WBM parameters for the hydrodynamic groundwater constant and  $C_{SRP}$ , while slightly different from the best performing parameters, still resulted in fairly good agreement with observations.

685

### 3.2 Open Source WBM Model evaluation





690 Above, we reviewed previously-published WBM validations. As none of the prior versions of WBM code have been released open source, it is important to validate the exact model structure in this first open source release. In this section, we evaluate results from a global open source WBM simulation that uses publically available data inputs, and provides a comprehensive selection of tracking outputs. The simulation ran for 270 hours on a Dell PowerEdge R510 with Intel Xeon processors (2.93 Gbps) and simulated 2.3M grid cells for 10 years following 10 years of spinup.

### 3.2.1 Model setup

695 Here we use a global 5-minute spatial resolution WBM simulation for validation. WBM is first initiated with a 10 year spinup to bring stocks to an equilibrium state. Results shown below are from simulated years 2000 – 2009. All model input datasets are listed in Table 5. All parameters are set to default values. The model initialization file used for this simulation is available from Grogan et al. (2022b).

**Table 5.** Model input datasets for WBM simulations presented here.

Input data type	Input data	Download link or website	Citation
River network	MERIT 5-minute river network	<a href="http://hydro.iis.u-tokyo.ac.jp/~yamada/MERIT_Hydro/">http://hydro.iis.u-tokyo.ac.jp/~yamada/MERIT_Hydro/</a>	Yamazaki et al. (2019)
Precipitation (daily)	MERRA 2 (prectotcorr variable)	<a href="https://gmao.gsfc.nasa.gov/reanalysis/MERRA-2/">https://gmao.gsfc.nasa.gov/reanalysis/MERRA-2/</a>	Gelaro et al. (2017)
Temperature (daily average)	MERRA 2	<a href="https://gmao.gsfc.nasa.gov/reanalysis/MERRA-2/">https://gmao.gsfc.nasa.gov/reanalysis/MERRA-2/</a>	Gelaro et al. (2017)
Dams & reservoirs	HydroConDams v2.0 for the continental US, and GrAND v1.3 for outside the continental US.	<a href="https://dataverse.harvard.edu/dataset.xhtml?persistentId=doi:10.7910/DVN/5YBWWI">https://dataverse.harvard.edu/dataset.xhtml?persistentId=doi:10.7910/DVN/5YBWWI</a> and <a href="https://globaldamwatch.org/grand/">https://globaldamwatch.org/grand/</a>	Lehner et al. (2011); Zuidema & Morrison (2020)
Soil available water capacity	Harmonized world soil database v1.2	<a href="https://www.fao.org/soils-portal/data-hub/soil-maps-and-databases/harmonized-world-soil-database-v12/en/">https://www.fao.org/soils-portal/data-hub/soil-maps-and-databases/harmonized-world-soil-database-v12/en/</a>	Fischer et al. (2008)
Root depth*	Effective rooting depth from Yang et al. (2016), gap-filled with the FAO/UNESCO digital soil map of the world v3.6	<a href="https://doi.org/10.4225/08/5837b3aa9cb90">https://doi.org/10.4225/08/5837b3aa9cb90</a> and <a href="https://www.worldcat.org/title/digital-soil-map-of-the-world-and-derived-soil-properties/oclc/52200846">https://www.worldcat.org/title/digital-soil-map-of-the-world-and-derived-soil-properties/oclc/52200846</a>	FAO/UNESCO (2003); Yang et al. (2016)



Glacier runoff, volume and area*	GloGEM glacier model		Huss & Hock (2015)
Crop maps & calendars*	MIRCA2000 v1.1	<a href="https://www.uni-frankfurt.de/45218023/MIRCA">https://www.uni-frankfurt.de/45218023/MIRCA</a>	Portmann et al. (2010)
SW:GW ratio*	FAO AQUASTAT	<a href="https://www.fao.org/aquastat/statistics/que-ry/index.html;jsessionid=71F6F6340C470CFBE92D71489546AA39">https://www.fao.org/aquastat/statistics/que-ry/index.html;jsessionid=71F6F6340C470CFBE92D71489546AA39</a>	FAO (2015)
Irrigation Efficiency	Rasterized data from Table 1 of Döll and Siebert (2002)	<a href="https://agupubs.onlinelibrary.wiley.com/doi/full/10.1029/2001WR000355">https://agupubs.onlinelibrary.wiley.com/doi/full/10.1029/2001WR000355</a>	Döll & Siebert (2002)
Rice paddy percolation rate*	Derived from the FAO/UNESCO soil map of the world	<a href="https://www.fao.org/soils-portal/soil-survey/soil-maps-and-databases/faunesco-soil-map-of-the-world/en/">https://www.fao.org/soils-portal/soil-survey/soil-maps-and-databases/faunesco-soil-map-of-the-world/en/</a>	FAO/UNESCO (2003), with derived data described by Wisser et al. (2008)

700 \*Primary data was processed for formatting, gap-filling, or to generate a calculated product; the resulting formatted files are provided for download at <https://wbm.unh.edu/> (Grogan et al., 2022) for simulation reproducibility.

### 3.2.2 Validation data and methods

705 *River discharge:* We validate WBM using default parameter values (Table 2) against daily and monthly river discharge records from the Global Runoff Data Centre (GRDC; [https://www.bafg.de/GRDC/EN/02\\_srvcs/21\\_tmsrs/riverdischarge\\_node.html](https://www.bafg.de/GRDC/EN/02_srvcs/21_tmsrs/riverdischarge_node.html)), which we downloaded in February of 2020. The GRDC user terms of agreement prohibits sharing of this data, but the same data can be requested directly from the GRDC.

710 GRDC stations were filtered based on three criteria. The first criteria is that the station must have data within the simulation time frame of years 2000 – 2009. The second criteria is that within the time frame, the station must have at least 12 observations for monthly validation, or at least 365 observations for daily validation. The third criteria compares the GRDC-reported catchment area of a station to the catchment area of the best-matching MERIT river network grid cell within a 3-by-3 grid centered on the latitude/longitude point defined by the GRDC station. Only GRDC stations with catchment area differences of less than 10%, once the best area match within the 3x3 grid is identified, are included. Applying these criteria  
 715 leaves 322 stations for daily and 344 stations for monthly validation.

We evaluate simulated daily and monthly average discharge with the Mean Bias Error (MBE), computed as:



$$MBE = \frac{1}{n} \sum_{i=1}^n P_i - O_i \quad (31)$$

720 Where  $P_i$  are predicted (i.e., simulated) discharge values,  $O_i$  are observed discharge values, and  $n$  is the number of observations. We also calculate the Index of Agreement,  $d$ , (Willmott, 1981):

$$d = 1 - \frac{\sum_{i=1}^n (O_i - P_i)^2}{\sum_{i=1}^n (|P_i - \bar{O}| + |O_i - \bar{O}|)^2} \quad (32)$$

which ranges in value from 0 for a model that is not a better predictor than the mean observed value, to 1.0 for a perfect match of predictions to observations.

725

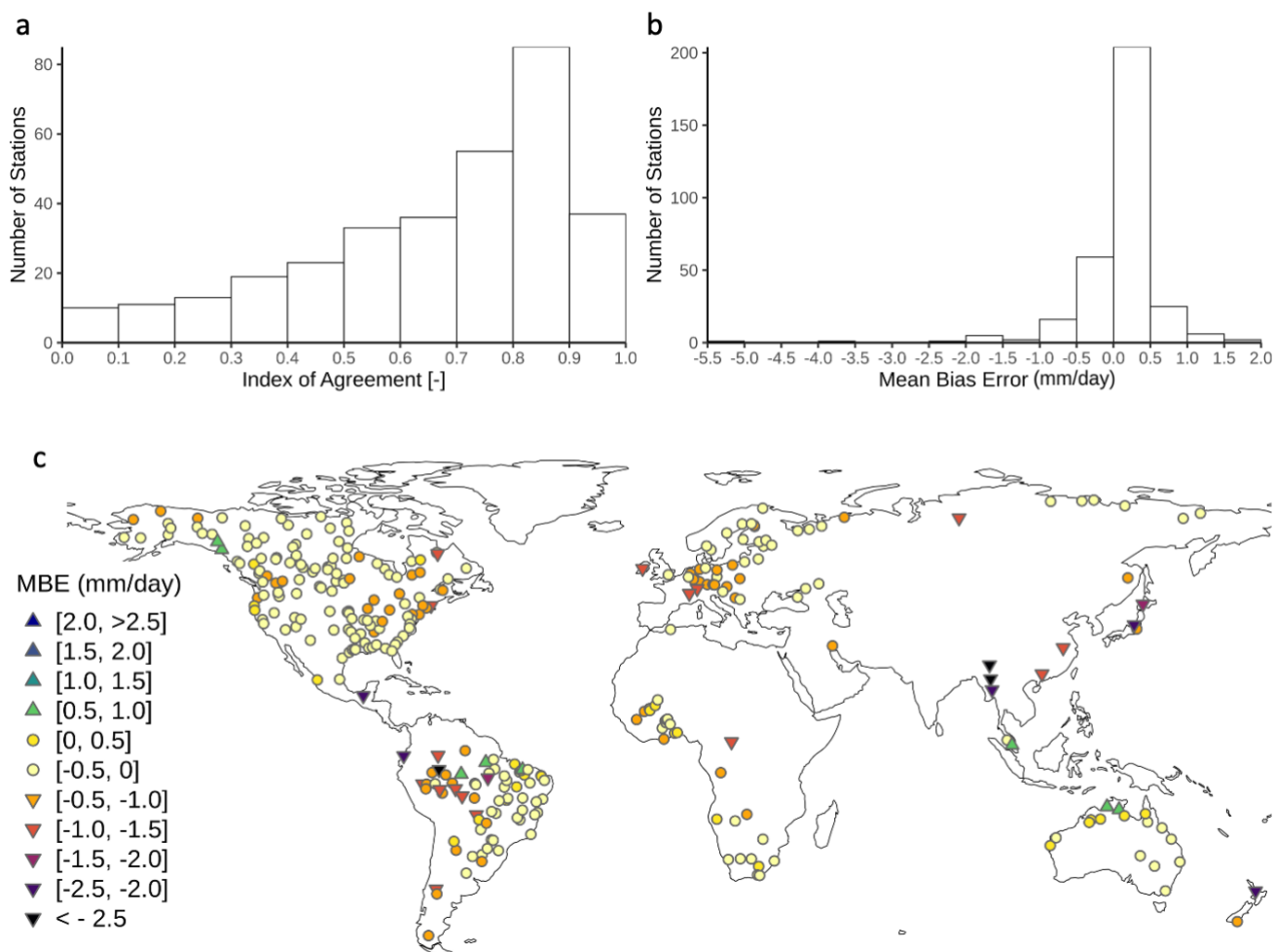
*Irrigation water withdrawals:* We compare WBM-simulated irrigation water withdrawals by source to reported country-level water withdrawal statistics from AQUASTAT (FAO, 2016), as well as other model-based estimates of withdrawal in the literature.

### 730 3.2.3 Results

*Daily river discharge:* Overall, global daily average discharge is simulated with moderate agreement to observations; the average index of agreement over all stations is 0.56, and average Mean Bias Error (MBE) is  $-0.07 \text{ mm day}^{-1}$  (Fig. 5a,b). However, there is substantial spatial variation in these metrics, with the mean highly influenced by the relatively large number of GRDC stations in the Americas compared to other continents. The lowest single river discharge MBE value is -  
735  $5.5 \text{ mm day}^{-1}$ , which occurs in Southeast Asia (Fig. 5b).

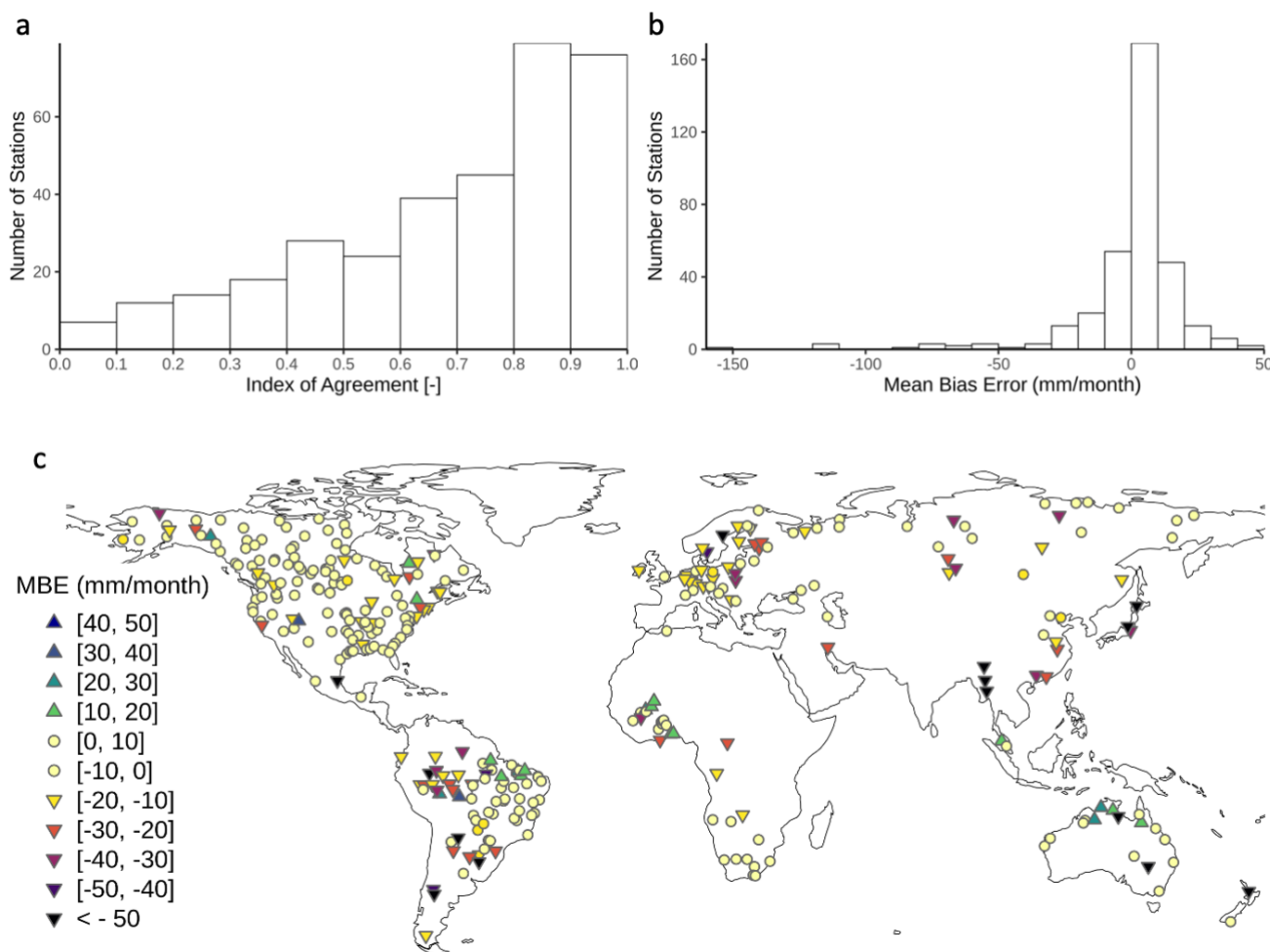
*Monthly river discharge:* Overall, global monthly average discharge is simulated with good agreement to observations; the average index of agreement over all stations is 0.69, and average Mean Bias Error (MBE) is  $-0.14 \text{ mm month}^{-1}$  (Fig. 6a,b). These results are consistent with Wisser et al. (2010a), even though different climate inputs and simulation time series were used.

740 Despite the global average good agreement, there is significant spatial variability, with lower MBE values across much of South America and East Asia (Figs. 5c and 6c). There are also notable large regions without any validation data that meet the criteria for inclusion in this analysis, including South Asia, Northern Africa, and the Middle East.



745

**Figure 5.** Frequency distribution of the Index of Agreement (a) and the Mean Bias Error (b, c) for daily average discharge. Average Index of Agreement is 0.56, and average MBE is  $-0.07 \text{ mm day}^{-1}$ .



750 **Figure 6.** Frequency distribution of the Index of Agreement (a) and the Mean Bias Error (b, c) for monthly average  
 discharge. Average Index of Agreement is 0.69, and average MBE is  $-0.14 \text{ mm month}^{-1}$ .

*Irrigation water withdrawals:* Simulated irrigation water withdrawals falls on the high end of previously-reported GHM-  
 simulated global irrigation water use (Table 6). Note that Wisser et al. (2008) demonstrated a large uncertainty in GHM-  
 755 simulated global irrigation water withdrawals as a function of input climate and crop map data. WBM simulations match  
 well to AQUASTAT (FAO, 2016) country-level statistics on agricultural water use (Fig. 7) for most countries, with an  $R^2$   
 value of 0.84 on a linear regression of country-year combinations included in both the AQUASTAT database and WBM  
 simulations. However, WBM simulates much higher irrigation water use in China and Pakistan than reported by  
 AQUASTAT (2 to 3 times higher), accounting for most (up to 90%) of the difference between WBM and the mean of other  
 760 GHM-simulated global agricultural water withdrawals (Table 6). As can be seen in Figures 5 and 6, river discharge across

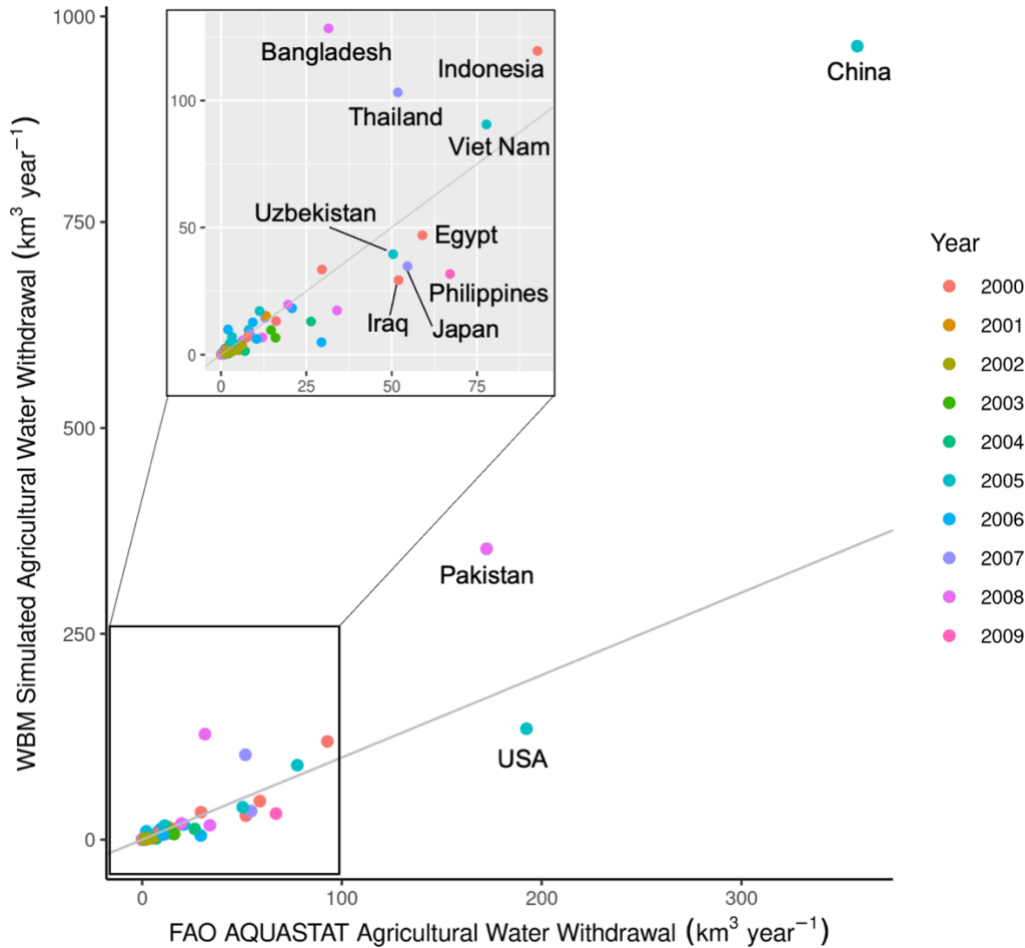


much of Asia is under-estimated by this WBM simulation; this is likely at least part of the reason for the over-estimation of irrigation water withdrawals in China and across much of Asia (Fig. 7).

**Table 6:** Previous global estimates of irrigation water withdrawal compared to this study's simulation.

	Source	Year	Value (km <sup>3</sup> year <sup>-1</sup> )
Total irrigation water withdrawal	Döll & Siebert (2002)	1961 – 1990	2,452
	Wisser et al. (2008)	2000	2,000 – 4,100
	Rost et al. (2008)	1971 – 2000	2,555
	Sulser et al. (2010)	2000	3,128
	Wada et al. (2011)	1958 – 2001	2,057
	Pokhrel et al. (2012)	2000	2,462 (± 130)
	Döll et al. (2014)	2003 – 2009	2,400
	Wada et al. (2014)	1979 – 2010	2,217 – 2,885
	Hanasaki et al. (2018)	2000	2,544 (± 75)
	Grogan et al. (2017)	2000	3,244 (± 240)
	Sutanudjaja et al. (2018)	2000 – 2015	2,309 – 2,735
	AQUASTAT (FAO, 2016)	2000	2,434
	This study*	2000 – 2009	3,889 (± 126)

765 \*Uncertainty estimate is the standard deviation of annual values from 2000 – 2009.



770 **Figure 7.** WBM-simulated irrigation water withdrawals compared to FAO AQUASTAT-reported values, by country. The 1:1 line is shown in grey. Countries with FAO-reported agricultural water withdrawals  $< 100 \text{ km}^3 \text{ year}^{-1}$  are shown in the inset. Countries with FAO-reported agricultural water withdrawals  $> 50 \text{ km}^3 \text{ year}^{-1}$  are labeled.

#### 4 Water source tracking module demonstration

775 WBM's unique water source tracking functions distinguish it from other GHMs. Here, we demonstrate the suite of tracking options available to model users: primary source tracking (4.1), return flow tracking (4.2), and land surface label tracking (4.3). Tracking output explains how the model arrives at simulated water stocks and flows. For example, river discharge is a collection of water flowing from different sources. These tracking functions make explicit what the sources are within the model that form the simulated discharge. We caution that any model can arrive at a well-validated result through erroneous

780 assumptions and aggregate errors. We find the component tracking increases the transparency of model assumptions; however, validation data for these tracking functions is not available at this time, and we rely on validation of the stocks and



785 fluxes themselves (not the component composition) for model evaluation. Future regional scale work could make use of  
emerging datasets on DNA or geochemistry such as chloride (Zuidema et al., 2018) to evaluate return flows from human and  
agricultural uses (Plummer et al., 2000), and stable water isotopic methods may be able to distinguish rain, snow melt, and  
glacier water sources ( Fekete et al., 2006; Fan et al., 2016; St Amour et al., 2005).

790 Here we use the same global, 5-minute spatial resolution WBM simulation as used for model validation to demonstrate the  
first two tracking examples: primary source tracking and the return flow tracking, as multiple tracking functions can be  
implemented within a single model run.

#### 4.1 Primary source tracking

795 The primary source tracking function identifies all water entering the model system as originating from one of four  
categories: rain, snow, glacier runoff, or unsustainable groundwater. Note that the shallow groundwater pool is filled with  
water from one of these categories, and so shallow groundwater and baseflow are not primary source categories. Glacier  
runoff, as taken from a glacier melt model such as GloGEM (Huss & Hock, 2015) or the more recent PyGEM (Rounce et al.,  
2020) includes all the water fluxes that occur on the glaciated area. This means that glacier runoff includes the rain,  
snowmelt, and glacier ice melt from the glacier area. Figures 8 and 9 show the fraction of average annual discharge (Fig. 8)  
and shallow groundwater (Fig. 9) composed of each of the primary sources, for each grid cell. Global discharge is dominated  
800 by rain over most of the globe, with snowmelt an important contributor at the poles, and both glacier runoff and  
unsustainable groundwater important regionally. The composition of shallow groundwater mirrors that of discharge. Due to  
human redistribution, water inputs to the land-surface can support streamflow and agriculture far from where they occurred,  
as can be seen in Figure 10, which shows the source, distribution, and use of glacier runoff. As can be seen in Figure 11,  
water sources like glacier runoff and unsustainable groundwater contribute to river flows, and therefore water resources, far  
805 downstream of where glacier runoff or pumped unsustainable groundwater is input to the river network. Figure 11 also  
shows how tracking can identify different contributions of source water to river flows through the year, as well as how  
glacier runoff is an important component of water supply far downstream in the basin late in the year.



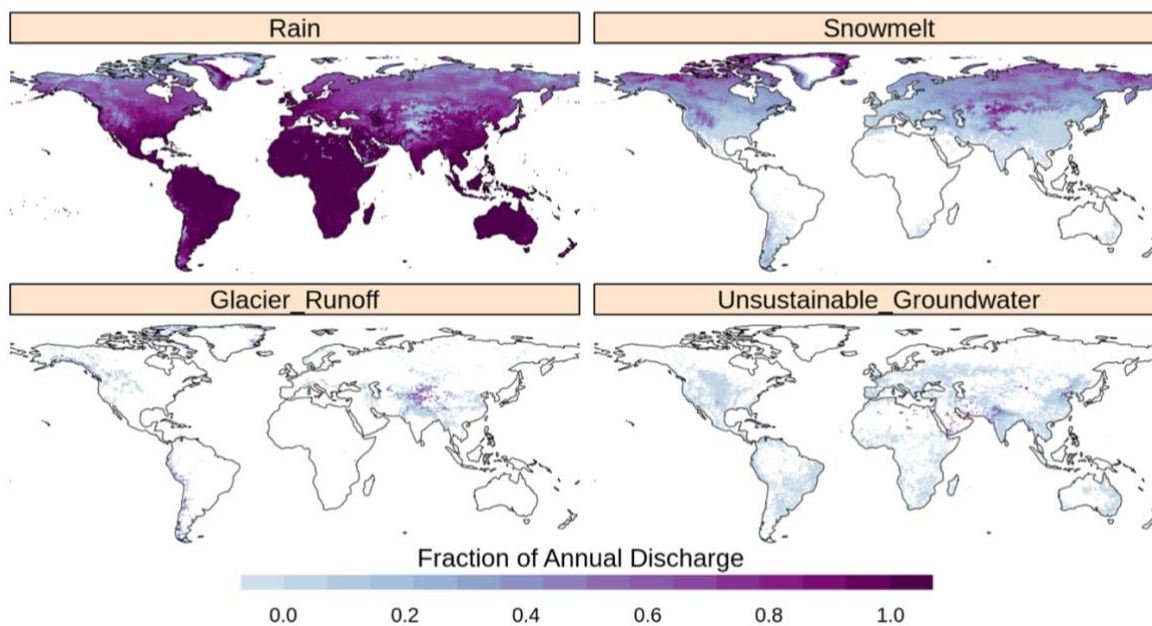


**Figure 8.** The fraction of annual average discharge composed of the four different primary source water components used in the primary source tracking method.

810

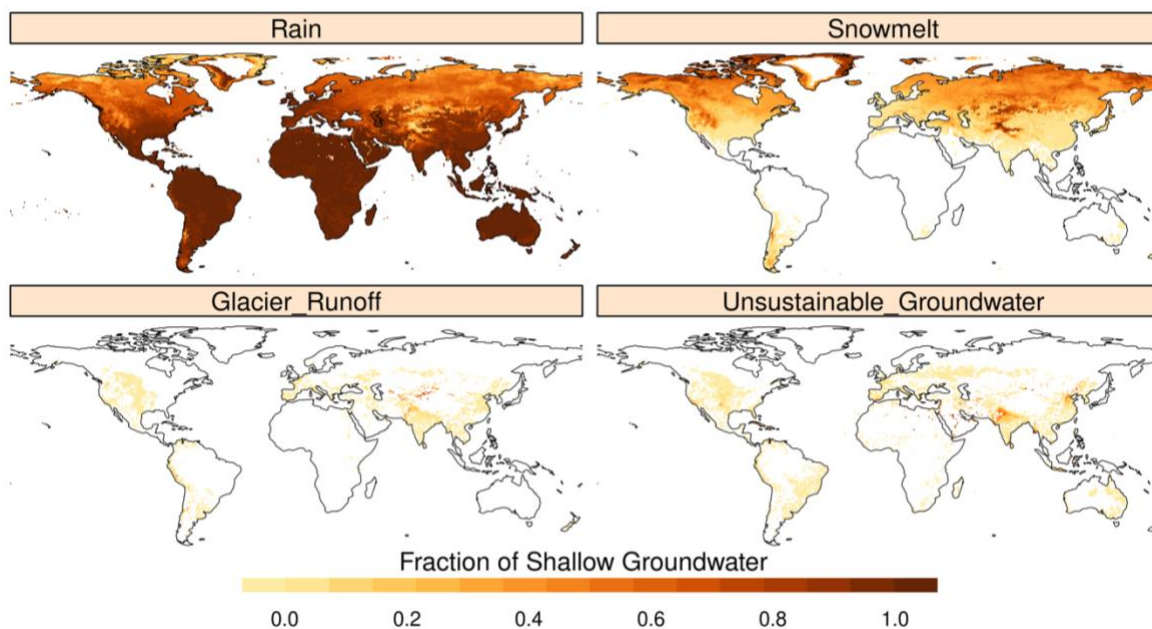
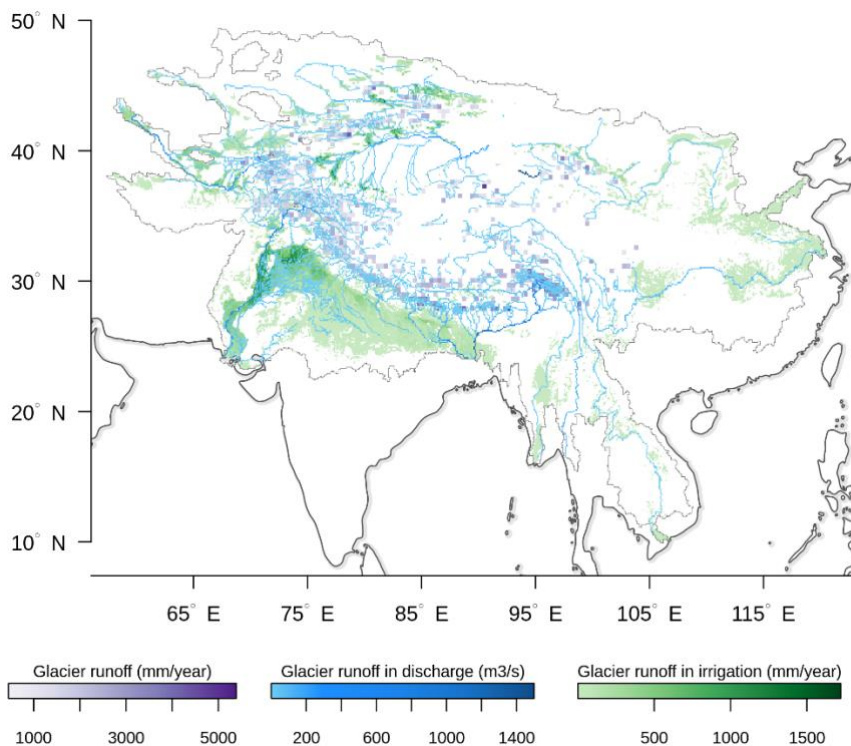


**Figure 9.** The fraction of annual average shallow groundwater storage composed of the four different primary source water components used in the primary source tracking method.



815

**Figure 10.** Tracking glacier runoff (purple) downstream through rivers (blue) and irrigation water use (green) in High Mountain Asia, a region where glacier meltwater is an important resource. While glacier water originates in the mountains, its use in agriculture is extensive due to reuse through the river network and shallow groundwater stores, and retention in and distribution from large reservoirs. The boundary of all High Mountain Asia basins with glaciers at their headwaters is shown in grey.

820

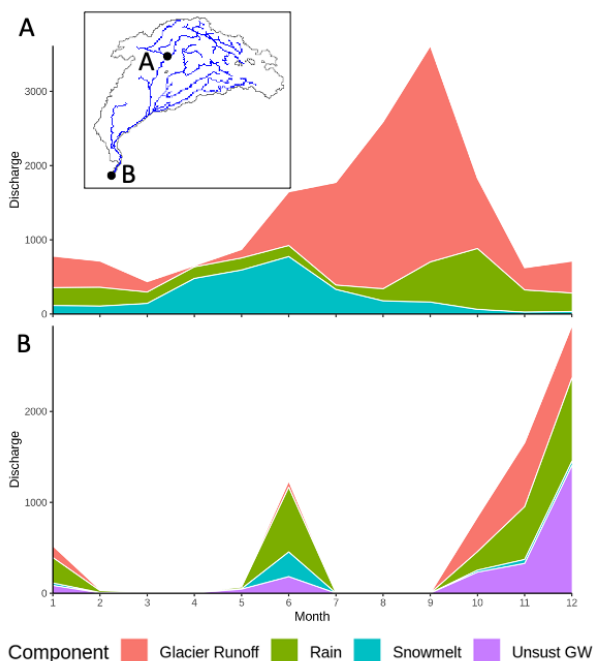


**Figure 11.** Monthly discharge by primary source component at two points (A, B) along the Indus River (basin shown in inset). Point A is in the headwaters, with substantial contributions from snowmelt and glacier runoff. Point B is the river mouth. The mouth of the Indus River runs dry in this simulation due both the seasonality of precipitation in the monsoonal region, and the large amounts of water extracted from the river for use. This use and re-use of water can be seen in the distribution of primary water sources remaining at the mouth of the river, which include unsustainable groundwater (purple) that was pumped from upstream sources, as well as snowmelt (blue) and glacier runoff (red), both of which are generated far upstream of the river mouth.

845

850

#### 4.2 Return flow tracking

855

The return flow tracking function labels water that flows back to the system after being extracted for irrigation, livestock watering, domestic, or industrial use. Irrigation return flows are identified separately from water returned by other human uses, but returns from domestic, industrial, and livestock uses are not tracked individually (but rather are lumped into one return category) for parsimony. These return flows have water quality implications, and through this tracking function WBM can identify when a body of water is increasingly composed of water returned from anthropogenic activities. At the beginning of a simulation, all water is considered “relict”, which assumes no knowledge of the source of the water. New water entering the system during the simulation period as precipitation or glacier runoff is tagged as “pristine” water. This functionality was first published in (Zuidema et al., 2020).

860

Figure 12 shows the fraction of average annual discharge composed of irrigation return flows, and Figure 13 shows the fraction of irrigation water withdrawals composed of irrigation return flows (water reuse). These fractional values cannot



exceed 1, even as return flows are reused multiple times; when return flow water is extracted again for reuse, it simply retains its identity as return flow, and does not contain any new information on the number of times it has been extracted.

865 Return flows from all human water uses contribute to water quality issues, including excess nutrients from irrigation returns and pathogens from domestic and livestock returns, some proportion of which may be attenuated by the river network depending on flow conditions (Huang et al. 2022) before being used again. Further, reuse of return water is an important consideration in studies evaluating the ‘efficiency’ of irrigation or other abstractions. Management actions that decrease returns in one region may reduce water availability downstream, which may promote extraction of alternative and potentially

870 less sustainable sources of water (Grafton et al., 2018; Grogan et al., 2017).

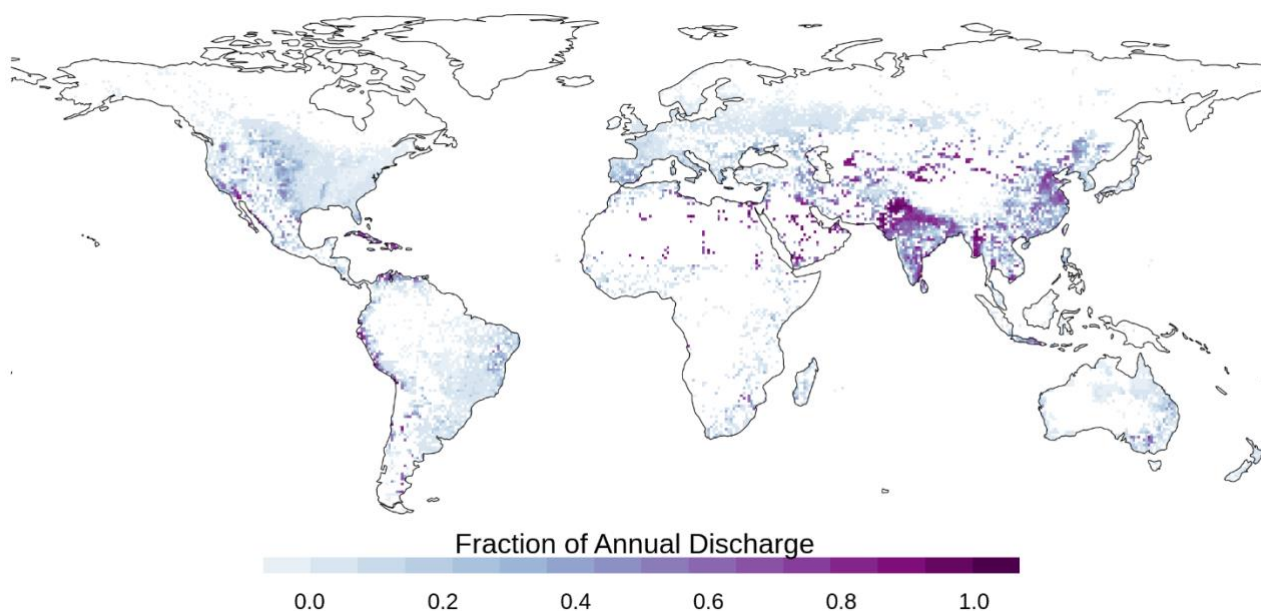
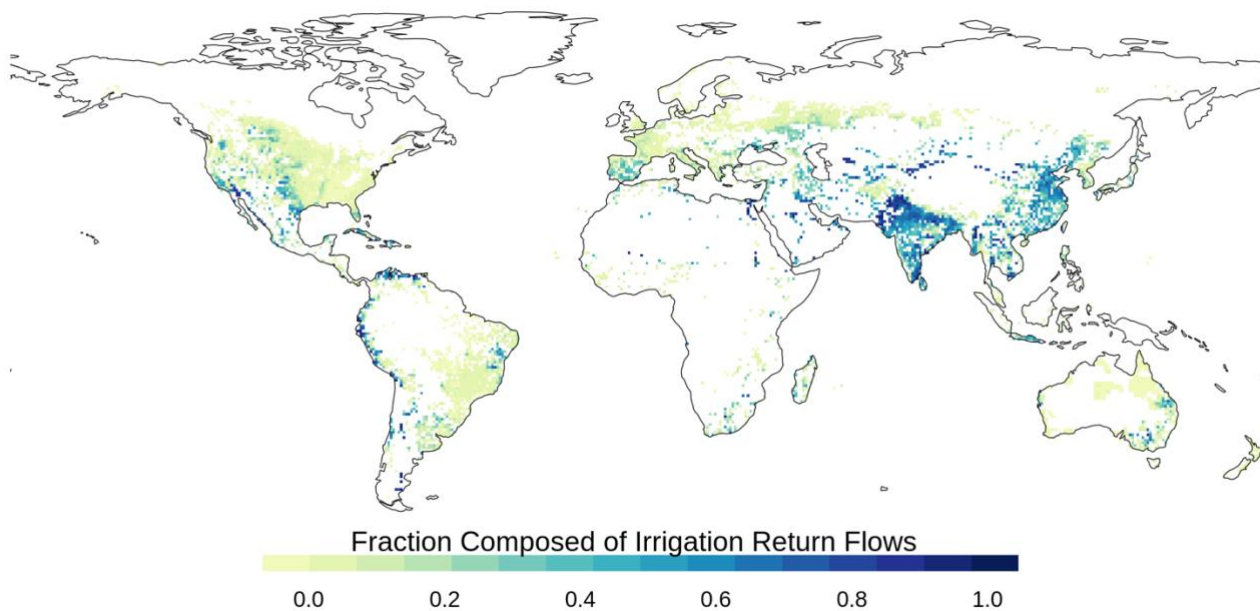


**Figure 12.** Fraction of average annual discharge composed of irrigation return flow water, simulated by the return flow tracking function.



875 **Figure 13.** Fraction of average annual irrigation withdrawals composed of prior irrigation returns simulated by return flow tracking function.

### 4.3 Land surface attribute tracking

#### 4.3.1 Model setup

880 Here we use the same set of model inputs and parameters as the global 5-minute spatial resolution WBM simulation described above, but reduce the spatial domain to only simulate grid cells downstream of headwaters in the U.S. state of Wyoming. One additional model input is required for the land surface attribute tracking: identification of which grid cells are within each of the U.S. states that intersect the spatial domain. This input (which includes a gridded file and an accompanying attribute text file) allows WBM to track water that originates as runoff within each U.S. state as it travels  
885 downstream through four major river basins (the Mississippi, Columbia, Colorado, and Great Basin) which span both sides of the continental divide. Applications of this technique would be useful for research involving transboundary conditions in river basins or using land cover masks to understand urban/rural or forest/non-forest effects in regional hydrology.

#### 4.3.2 Results

890 Tracking runoff generated by different U.S. states demonstrates how the land surface attribute tracking can be used to identify contributions of water from any user-identified spatial attributes. The basins simulated here all contain cities and both extensive and intensive irrigated areas; the land surface attribute tracking maintains the U.S. state identification of all surface and shallow groundwater withdrawals and return flows as water travels through the system from headwaters to river



895 outlets. Figure 14a illustrates how this tracking is useful for identifying multiple land attribute contributors to river discharge at a point. Figure 14b demonstrates the spatial distribution of water from one land attribute through many downstream systems. Particularly in Figure 14b we can see how human extractions of water – which can occur across grid cells – spreads the tracked land attribute’s contributed water across the landscape.

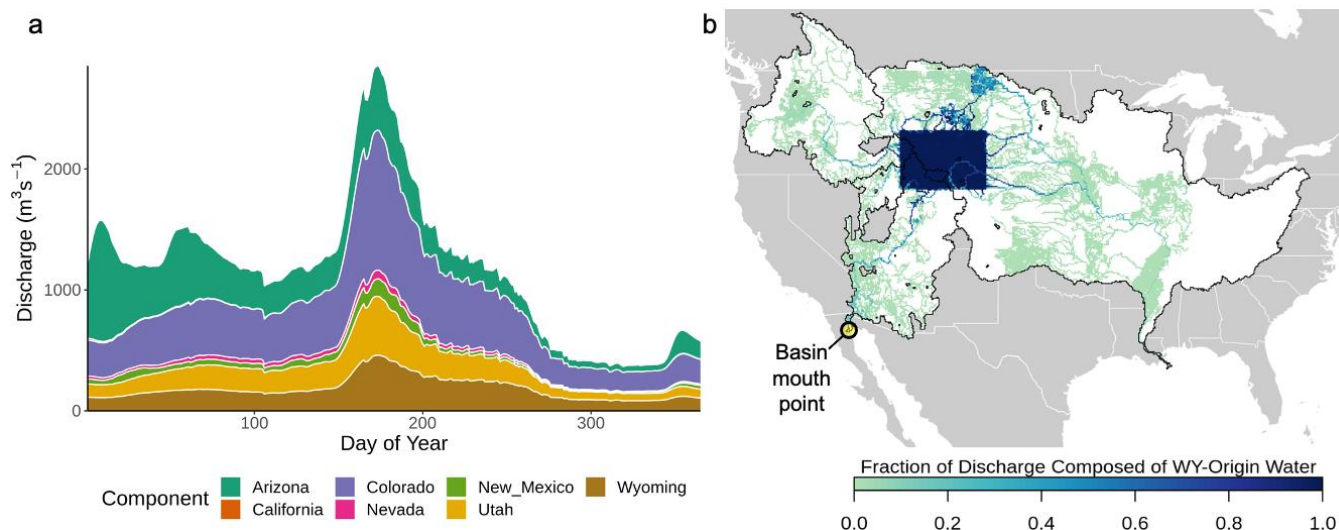


**Figure 14.** Demonstration of WBM’s land surface attribute tracking function: (a) Discharge at the mouth of the Colorado River Basin (basin mouth point shown in panel b). Colors show contribution of water from seven different U.S. states, accounting for the movement, storage, and cycles of extraction occurring across the basin’s many upstream water uses. (b) Fraction of Wyoming state waters in river discharge on July 1, 2009. Basins in the study domain are outlined in black; grey regions are not simulated.

## 905 5 Model code

*Brief history of model code development:* WBM was originally written in FORTRAN, and first published in (Vörösmarty et al., 1989). The first publication described WBM as a continental-scale model of water balance and fluvial transport, and presented an application to South America. The first global applications were published in (Vörösmarty et al., 1998) and (Vörösmarty et al., 2000a). Over its 30+ year history of development, WBM has been re-written in several programming languages, and branches have been developed for specific applications (Table 7). Table 7 describes each branch of WBM, with its acronym (e.g., WBM vs. PWBM), the application for which the branch was developed, and key publications. Many of the branches are still in use by a variety of research groups, including researchers at The University of New Hampshire (WBM\*), City College of New York (WBM), University of Alabama (WBMsed), and University of Massachusetts (PWBM).

915



**Table 7.** Major WBM code branches, along with their history of new functionality and if the code branch is still in use.

Model full name	Acronym	Language	New functions	Key publications	In use
Water Balance Model	WBM	FORTRAN	Original: continental to global scale water balance	D’Almeida et al. (2006); Vörösmarty et al. (1989)	No
Water Balance Model	WBM	C/C++	Original: continental to global scale water balance	Fekete et al. (2002); Vörösmarty et al. (1998 2000, 2005, 2010)	Yes
Pan-Arctic Water Balance Model	P/WBM and PWBM	FORTRAN	Added permafrost functions for pan-arctic applications	Rawlins et al. (2003, 2005); Rawlins et al. (2006a,b)	Yes
Framework for Aquatic Modeling of the Earth System	FrAMES	C++	Constituent fluxes into river systems, accounting for transport and fate of nitrogen, chloride, and E. coli  Water temperature	Miara et al. (2017, 2019); Miara & Vörösmarty (2013); Mineau et al. (2015); Samal et al. (2017); Stewart et al. (2011b; 2013); Wollheim et al. (2008a,b); Wollheim et al. (2015); Zuidema et al. (2018) Huang et al. (2022)	Yes
Water Balance Model plus	WBMplus	C++	Irrigated agriculture and reservoirs	Wisser et al. (2008); Wisser et al. (2010a,b)	No
WBM sediment	WBMsed	C++	Sediment transport	Cohen et al. (2013, 2014); Dunn et al. (2019)	Yes
Water Balance Model*	WBM	Perl/PDL	Added rainfed agriculture, other land cover types, inter-basin transfers, domestic and livestock water demand, tracking.  Includes FrAMES functionality, and water temperature	Grogan (2016); Grogan et al. (2015, 2017, 2020); Haqiqi et al. (2021) Liu et al. (2017); Mishra et al. (2020); Webster et al. (2022) Zaveri et al. (2016); Zuidema et al. (2020) Grogan et al. (2022a)	Yes

\*This version of WBM is the open source model described in this paper.



920 *WBM Open Source code:* The WBM version described here is written in Perl/PDL. The coding language was changed from  
C++ to Perl/PDL by the University of New Hampshire research group in 2010 to make use of PDL functionality that was  
unique to that language at the time, namely:

- 1) Efficient parallel processing of matrix operations on large spatial matrices allowing increased computational  
performance similar to than C or Fortran through the use of binary PDL operators/functions and multithreading,
- 925 2) Adding pre-compiled custom functions written in inline C (PDL PP modules), and
- 3) Fully integrating the river transport module with the land surface component of WBM to simulate the full  
downstream effects of water withdrawals from the rivers. Prior versions of WBM resolved the time component  
prior to the spatial component of the model; this prevented implementation of water extractions and inter-basin  
transfers.

930 The open source Perl/PDL version of WBM described here includes all the functionality of the original FORTRAN WBM  
model, the WBMplus model, and some aspects of the FrAMES model. All model branches run on Linux operating systems.  
The open source WBM code described here is composed of three main files: `wbm.pl`, which is the main model script;  
`WBM.pm`, a module providing WBM specific functionality; and `RIMS.pm`, a module providing geospatial and temporal  
transformation utilities. The entire modeling framework is dependent upon other software: perl, PDL, gdal, ogr, and  
935 NetCDF. The model input data repository (<https://wbm.unh.edu/>, Grogan et al., 2022) also includes a Singularity container  
which has pre-installed the required operating system and software dependencies for ease of model use by the research  
community.

WBM can run high density grids in a simulation domain up to about 3 million active grid cells on an average rack system  
940 server and utilize CPU parallelization (multi-threading) for a performance boost. Smaller spatial domains can be run on a  
personal desktop or laptop computer.

*Code implementation:* WBM is rasterized and generally used with uniformly spaced gridded data data, keeping values of  
gridcell-specific area in memory for flux calculations. The model is modular, with many options to turn on or off irrigation  
945 and other human water extractions. Options are controlled by the user through a selection of direct inputs, on/off flags, and  
output variables requested of the model. WBM employs a split-operator method for calculating changes in stocks as a  
function of sequential fluxes. Stocks and fluxes including irrigation demand, evapotranspiration, and runoff generation are  
calculated in the first portion of the time-step loop utilizing vectorized and efficient array utilities of the perl Data Language.  
Water entering stream reaches throughout the network is then submitted to a routing function that traverses a directed,  
950 noncyclical graph of all grid cells that ensures an upstream-to-downstream calculation order, written in an inline, pre-  
compiled format to maximize computational efficiency. In a number of areas, the model makes use of split-operator  
solutions to facilitate both tracking functionality and the complex interactions between human water withdrawals and natural





955 systems. This simple method allows WBM to re-calculate water stocks and fluxes after water extraction occurs and again after return flows, such that the final stock and flux values at the end of a time step are modified from the first instance of calculation at the beginning of the time step. As noted by others, leveraging of split-operator solutions for hydrologic models provides a tradeoff between efficiency and accuracy in numerical solutions, which is warranted in some cases (Clark et al., 2015).

*How to use WBM:* The WBM workflow involves 5 basic steps:

- 960
- 1) Prepare input data, metadata, and parameter files
  - 2) Write a model setup file with the extension “*.init*”
  - 3) Test setup file by running WBM with flags “-test”, “-noRun”, and “-err”.
  - 4) Execute the model code (wbm.pl)
  - 5) Perform post-processing, if needed, with automatically generated utilities for temporal aggregation of select or all
- 965 output variables.

A detailed instruction manual is included in the model’s github repository, along with perl utilities commonly used in steps 1 and 5.

970 In Step 1, the model user must collect all input data required for the given model simulation. Each spatial data set and database must be described in a metadata file with the extension “*.init*”. All data and model input “*.init*” files are simple text files with formatting that conforms to a perl hash. Input file unit conversions (e.g., converting temperature data from °C to °F) do not need to be performed prior to running WBM. Rather, the user can define a conversion slope and intercept for linear transformations within the metadata “*.init*” files, and WBM will automatically calculate the new units through the RIMS.pm module.

975 In Step 2, the model user writes a model setup file with the extension “*.init*” that lists all model inputs as well as other key parameters such as the start year, end year, list of output variables to save, and output directory location. This setup file points directly to the input data *.init* metadata files, and includes options to directly define parameter values and set binary on/off flags for particular modules. Most important is the identification of the digital river network. The input river network file determines the model simulation grid spatial resolution, spatial extent, projection, and defines non-land grid cells (which are set to a no data value). Other input datasets will automatically be clipped (extent reduced) and re-gridded (either through resampling or aggregation) to match the extent and grid cell resolution of the input river network file. This means that the model user does not need to do these spatial transformations prior to starting the model.

985 In Step 3, the user tests the model setup and produces an optional input data pre-processing script. Test mode and “noRun” mode call the input data reading functions from RIMS.pm and set up the model run’s output directory. This step is used to



990 identify any errors in the model setup, which are commonly issues such as incorrect file paths, syntax errors in the “.init”  
files, or formatting errors in the raw data files. Executing wbm.pl in test and noRun mode also automatically generates a  
custom build\_spool.pl script (written to the model run’s output directory) that can optionally be executed prior to Step 4 to  
pre-process all input data files that require requisite spatial clipping, re-gridding, or unit conversions. If build\_spool.pl is  
executed, the results of input data pre-processing are saved as binary files that are read directly by WBM; these files can also  
optionally be saved as netCDF files for ease of analysis, so the user can evaluate the results of the processing step. If the  
custom build\_spool.pl script is not executed prior to starting the model in Step 4, it will automatically be executed in the  
model’s run time. Note, this automatic option only produces binary files, and does not output any netCDF files. The  
995 build\_spool.pl utility can leverage multiple CPUs to efficiently build binary input files; the automatic option processes all  
binary files in a single process with a steep reduction in model simulation time.

1000 In Step 4, the model user executes wbm.pl via direct command line entry. The code wbm.pl has several flag options,  
including -h for help, -v for verbose mode, and others described in the instruction manual. The model setup file is the only  
required argument to wbm.pl. Under verbose mode, detailed statistics of model run time, global aggregate water balances,  
and water supply metrics are reported to the user during each time-step, with more complete accounting of water balances  
reported at the end of each year of the simulation. Model run state files are written at the end of spin-up, and at the end of  
each year, and (optionally) more frequently. This frequent saving of state files enables users to re-start simulations in the  
event of an interruption (e.g., from power loss) without losing significant wall-time. Model output files are written in the  
1005 same spatial resolution and domain as the input digital river network.

Step 5 is the most application- and user-specific. The raw daily model output is rarely the final product of analysis; temporal  
and spatial aggregation or point-location time series extraction are most commonly required to evaluate output and produce  
research results. The model automatically generates daily-to-monthly and daily-to-yearly temporal aggregations, and the  
1010 setup file has a binary on/off option that enables automatic temporal aggregation to climatology (daily, monthly and yearly)  
averages using either the entire simulation period or specified year groups for averaging; there is also an input field for  
automatic spatial aggregation. Perl utilities for these operations are included in the model github repository.

## 6 Discussion

1015 WBM’s tracking functionality opens unique options for model-based experimentation with potentially important  
management implications within a GHM. Oftentimes, hydrologic modeling studies provide insight to the relative importance  
or effect of a particular hydrologic process by switching processes on and off, thereby creating slightly different systems.  
These studies identify the role of a specific process in a system by comparing two or more structural or parametric model  
configurations with and without representation of a particular process. Such analogies are most powerful when used to  
1020 understand the effect of hydrologic fluxes which are expected to fundamentally change such as glacial melt (Rounce et al.,



2020), or have been historically absent in previous hydrologic modeling such as surface depressions (Rajib et al., 2020). Similar approaches may test the effectiveness of different management strategies, such as the effect of managed aquifer recharge on aquifer head and river flow (Niswonger et al., 2017; Tran et al., 2019; Van Kirk et al., 2020; Zuidema et al., 2020). In other cases, this approach has been used to assess the difference between a hypothetical natural system (with no human impacts) and a human-impacted system (Wada et al., 2016).

By using the tracking methods described here, it is possible to attribute a portion of water flows to a specific process, location, water source, or flow-path, without altering the represented system from an existing or experimental configuration. This is fundamentally different from the on/off method of evaluating process or source importance that has been more commonly used in the literature. WBM's tracking module achieves this by attributing the water stored and moving between each pool within each grid cell a composition of processes or water sources that brought that water to a point in space and time. For example, this tracking function facilitates calculation of irrigation returns in future withdrawals that make estimation of effective irrigation efficiency (Haie & Keller, 2008) possible under suites of hypothetical management configurations (Zuidema et al. 2020).

As described in (Weiler et al., 2018), several different water tracking methods have been employed by regional hydrologic models, though as of this writing, no global hydrologic model other than WBM employs these types of tracking methods. Regional hydrologic model tracking methods include synthetic scalar transport, solute transport, particle tracking, and the "effective tracking" used in HBV-Light (Stahl et al. 2017, Weiler et al. 2018) . WBM's (Weiler et al., 2018) tracking fits into the class of "effective tracking" methods described by Weiler et al. (2018), and is a simplified version of the synthetic scalar transport method, analogous to solute transport where mixing within compartments of the model is substituted for a full calculation of the advection-dispersion equation. Insights provided by effective tracking into the sources of discharge and water provisioning are most relevant for evaluating human water resources (Weiler et al. 2018).

## 7 Conclusions and future work

The open source global hydrologic model WBM represents not only the natural terrestrial hydrologic system, but also human interactions with water resources. These interactions include hydro-infrastructure and water extractions for use by irrigation, livestock, domestic, and industrial sectors. WBM provides a novel water component tracking functionality that enables GHMs for the first time to attribute the influence of different water sources and flow paths on stocks and fluxes such as river discharge or irrigation water supply. Tracking illustrates the importance of teleconnections between input sources and human uses, such as the withdrawal of glacier water far downstream, or the extraction of agricultural returns for subsequent reuse. It does this by calculating the impact of water introduced by a flux without the need to estimate the effects by altering the system through their absence, which is critical for understanding how we interpret how the system is, rather than how a similar system might be. Evaluation of the global model shows good agreement with observed river discharge and water



1055 extractions, though the validation metrics have large spatial variability that highlights the need for parameter calibration  
when using WBM for regional analyses. As there are no equivalent empirical analogues, evaluating the tracking component  
compositions of any flux is not presently possible; however, tracking functionality creates a more transparent representation  
of the assumptions that drive model results. On-going development of WBM focuses on modules that improve the  
representation of human interactions with the water cycle, increased temporal resolution options, and data assimilation  
1060 functionality for use in operational forecasts.

### Code and data availability

WBM v1.0.0 is open source and distributed under the terms of the GNU Public License version 3, as published by the Free  
Software Foundation. Model code is provided in a GitHub repository: <https://github.com/wsag/WBM>, and release v1.0.0 is  
1065 archived on Zenodo (Grogan and Zuidema, 2022, <https://zenodo.org/record/6263097#.Yhhvk5PMKRrs>). Input data required  
to reproduce the simulations presented here that cannot be directly downloaded from other sources due to either lack of  
availability or substantial pre-processing requirements for use in WBM (see Table 5) are provided for download here:  
<https://wbm.unh.edu/> (Grogan et al., 2022; <https://dx.doi.org/10.34051/d/2022.2>). The GitHub repository will be updated as  
bug-fixes, new modules, and further development occurs. Development and maintenance of the main branch of WBM  
1070 continues at the University of New Hampshire, but we welcome contributions from other parties.

### Author contributions

DG contributed to conceptualization, methodology, formal analysis, validation, visualization, and original draft writing. SZ  
contributed to software development, data curation, and draft writing. AP contributed to software development,  
1075 investigation, data curation, and draft writing. SG contributed to software development (lead developer), investigation, and  
data curation. RL contributed to conceptualization, funding acquisition, project administration, supervision, writing – review  
& editing. WW contributed to funding acquisition, project administration, supervision, and manuscript.

### Competing interests

1080 The authors declare no competing interests.

### Acknowledgements

This work was supported by: The U.S. Department of Energy, Office of Science, Biological and Environmental Research  
Program, Earth and Environmental Systems Modeling, MultiSector Dynamics under Grant DE-SC005171 and Cooperative  
1085 Agreements DE-SC0016162 and DE-SC0022141. The National Science Foundation Division of Earth Sciences grant no.  
10388018; Division of Social and Economic Sciences grant no. 1639524; Division of Chemical, Bioengineering,  
Environmental, and Transport Systems grant no. 1855937; Division of Behavioral and Cognitive Sciences grant no.  
1114851; NH EPSCoR New England Sustainability Consortium grant no. EPS-1330641; NH EPSCoR Ecosystems and



1090 Society grant no. EPS-1101245; the Plum Island Long Term Ecological Research site grant no. OCE-1637630; and the  
Graduate Research Fellowship Program grant no. DGE-0913620. The National Aeronautical and Space Administration,  
Earth Science Division's High Mountain Asia program grant no. NNX17AB28G and grant no. 80NSSC20K1595 and the  
Earth Science Division's Sea Level Change program grant no. 80NSSC20K1296. The United States Environmental  
Protection Agency, Science to Achieve Results (R836169), Assessing the Contribution of Small Streams to Use and Non-use  
WaterQuality Values Using Modeling, Stakeholder Participation, and Decision Theory. The Swedish funding agency Formas  
1095 under grant #2017-00,608 via Stockholm University.

## References

- Aber, J. D., Ollinger, S. V., & Driscoll, C. T. (1997). Modeling nitrogen saturation in forest ecosystems in response to land use and atmospheric deposition. *Ecological Modelling*, *101*(1), 61–78. [https://doi.org/10.1016/S0304-3800\(97\)01953-4](https://doi.org/10.1016/S0304-3800(97)01953-4)
- 1100 Alexander, R. B., Boyer, E. W., Smith, R. A., Schwarz, G. E., & Moore, R. B. (2007). The Role of Headwater Streams in Downstream Water Quality 1: The Role of Headwater Streams in Downstream Water Quality. *JAWRA Journal of the American Water Resources Association*, *43*(1), 41–59. <https://doi.org/10.1111/j.1752-1688.2007.00005.x>
- Allen, R. G., Pereira, L. S., Raes, D., & Smith, M. (1998). FAO Irrigation and Drainage Paper. *Food and Agricultural Organization of the United Nations*, 333.
- 1105 Alley, W. M., & Veenhuis, J. E. (1983). Effective Impervious Area in Urban Runoff Modeling. *Journal of Hydraulic Engineering*, *109*(2), 313–319. [https://doi.org/10.1061/\(ASCE\)0733-9429\(1983\)109:2\(313\)](https://doi.org/10.1061/(ASCE)0733-9429(1983)109:2(313))
- van Beek, L. P. H., Eikelboom, T., Vliet, M. T. H., & Bierkens, M. F. P. (2012). A physically based model of global freshwater surface temperature. *Water Resources Research*, *48*(9), 2012WR011819. <https://doi.org/10.1029/2012WR011819>
- 1110 Biemans, H., & Siderius, C. (2019). Advances in global hydrology–crop modelling to support the UN's Sustainable Development Goals in South Asia. *Current Opinion in Environmental Sustainability*, *40*, 108–116. <https://doi.org/10.1016/j.cosust.2019.10.005>
- Bosmans, J. H. C., van Beek, L. P. H., Sutanudjaja, E. H., & Bierkens, M. F. P. (2017). Hydrological impacts of global land cover change and human water use. *Hydrology and Earth System Sciences*, *21*(11), 5603–5626. <https://doi.org/10.5194/hess-21-5603-2017>
- 1115 Bring, A., Shiklomanov, A., & Lammers, R. B. (2017). Pan-Arctic river discharge: Prioritizing monitoring of future climate change hot spots: PAN-ARCTIC RIVER DISCHARGE MONITORING. *Earth's Future*, *5*(1), 72–92. <https://doi.org/10.1002/2016EF000434>
- 1120 Clark, M. P., Nijssen, B., Lundquist, J. D., Kavetski, D., Rupp, D. E., Woods, R. A., et al. (2015). A unified approach for process-based hydrologic modeling: 1. Modeling concept. *Water Resources Research*, *51*(4), 2498–2514. <https://doi.org/10.1002/2015WR017198>
- Cohen, S., Kettner, A. J., Syvitski, J. P. M., & Fekete, B. M. (2013). WBMsed, a distributed global-scale riverine sediment flux model: Model description and validation. *Computers & Geosciences*, *53*, 80–93. <https://doi.org/10.1016/j.cageo.2011.08.011>



- 1125 Cohen, S., Kettner, A. J., & Syvitski, J. P. M. (2014). Global suspended sediment and water discharge dynamics between 1960 and 2010: Continental trends and intra-basin sensitivity. *Global and Planetary Change*, 115, 44–58. <https://doi.org/10.1016/j.gloplacha.2014.01.011>
- Cohen, S., Praskievicz, S., & Maidment, D. R. (2018). Featured Collection Introduction: National Water Model. *JAWRA Journal of the American Water Resources Association*, 54(4), 767–769. <https://doi.org/10.1111/1752-1688.12664>
- 1130 Dalin, C., Wada, Y., Kastner, T., & Puma, M. J. (2017). Groundwater depletion embedded in international food trade. *Nature*, 543(7647), 700–704. <https://doi.org/10.1038/nature21403>
- D’Almeida, C., Vörösmarty, C. J., Marengo, J. A., Hurtt, G. C., Dingman, S. L., & Keim, B. D. (2006). A water balance model to study the hydrological response to different scenarios of deforestation in Amazonia. *Journal of Hydrology*, 331(1–2), 125–136. <https://doi.org/10.1016/j.jhydrol.2006.05.027>
- 1135 Deardorff, J. W. (1978). Efficient prediction of ground surface temperature and moisture, with inclusion of a layer of vegetation. *Journal of Geophysical Research*, 83(C4), 1889. <https://doi.org/10.1029/JC083iC04p01889>
- Dee, D. P., Uppala, S. M., Simmons, A. J., Berrisford, P., Poli, P., Kobayashi, S., et al. (2011). The ERA-Interim reanalysis: configuration and performance of the data assimilation system. *Quarterly Journal of the Royal Meteorological Society*, 137(656), 553–597. <https://doi.org/10.1002/qj.828>
- 1140 Dickinson, R. E. (1984). Modeling evapotranspiration for three-dimensional global climate models. In J. E. Hansen & T. Takahashi (Eds.), *Geophysical Monograph Series* (Vol. 29, pp. 58–72). Washington, D. C.: American Geophysical Union. <https://doi.org/10.1029/GM029p0058>
- Digital soil map of the world and derived soil properties. (2003). [Electronic resource]. Rome, Italy: FAO.
- Dillon, P., Stuyfzand, P., Grischek, T., Lluria, M., Pyne, R. D. G., Jain, R. C., et al. (2019). Sixty years of global progress in managed aquifer recharge. *Hydrogeology Journal*, 27(1), 1–30. <https://doi.org/10.1007/s10040-018-1841-z>
- 1145 Dingman, S. L. (2002). *Physical hydrology* (2nd ed). Upper Saddle River, NJ: Prentice Hall.
- Dingman, S. Lawrence. (1972). Equilibrium temperatures of water surfaces as related to air temperature and solar radiation. *Water Resources Research*, 8(1), 42–49. <https://doi.org/10.1029/WR008i001p00042>
- Dingman, S.L. (2009). *Fluvial Hydraulics*. New York, NY: Oxford University Press.
- 1150 Döll, P., Hoffmann-Dobrev, H., Portmann, F. T., Siebert, S., Eicker, A., Rodell, M., et al. (2012). Impact of water withdrawals from groundwater and surface water on continental water storage variations. *Journal of Geodynamics*, 59–60, 143–156. <https://doi.org/10.1016/j.jog.2011.05.001>
- Döll, Petra, & Siebert, S. (2002). Global modeling of irrigation water requirements: GLOBAL MODELING OF IRRIGATION WATER REQUIREMENTS. *Water Resources Research*, 38(4), 8-1-8–10. <https://doi.org/10.1029/2001WR000355>
- 1155 Döll, Petra, Müller Schmied, H., Schuh, C., Portmann, F. T., & Eicker, A. (2014). Global-scale assessment of groundwater depletion and related groundwater abstractions: Combining hydrological modeling with information from well observations and GRACE satellites. *Water Resources Research*, 50(7), 5698–5720. <https://doi.org/10.1002/2014WR015595>
- 1160 Dottori, F., Szwedczyk, W., Ciscar, J.-C., Zhao, F., Alfieri, L., Hirabayashi, Y., et al. (2018). Increased human and economic losses from river flooding with anthropogenic warming. *Nature Climate Change*, 8(9), 781–786. <https://doi.org/10.1038/s41558-018-0257-z>



- 1165 Douglas, E. M., Chomitz, K. M., Sebastian, K., Vorosmarty, C. J., & Wood, S. (2005). *The Role Of Tropical Forests In Supporting Biodiversity And Hydrological Integrity: A Synoptic Overview*. The World Bank. <https://doi.org/10.1596/1813-9450-3635>
- Douglas, E. M., Niyogi, D., Frohling, S., Yeluripati, J. B., Pielke, R. A., Niyogi, N., et al. (2006). Changes in moisture and energy fluxes due to agricultural land use and irrigation in the Indian Monsoon Belt. *Geophysical Research Letters*, 33(14), L14403. <https://doi.org/10.1029/2006GL026550>
- 1170 Douglas, E. M., Wood, S., Sebastian, K., Vörösmarty, C. J., Chomitz, K. M., & Tomich, T. P. (2006). Policy implications of a pan-tropic assessment of the simultaneous hydrological and biodiversity impacts of deforestation. *Water Resources Management*, 21(1), 211–232. <https://doi.org/10.1007/s11269-006-9050-2>
- Dunn, F. E., Darby, S. E., Nicholls, R. J., Cohen, S., Zarfl, C., & Fekete, B. M. (2019). Projections of declining fluvial sediment delivery to major deltas worldwide in response to climate change and anthropogenic stress. *Environmental Research Letters*, 14(8), 084034. <https://doi.org/10.1088/1748-9326/ab304e>
- 1175 Eilander, D., van Verseveld, W., Yamazaki, D., Weerts, A., Winsemius, H. C., & Ward, P. J. (2021). A hydrography upscaling method for scale-invariant parametrization of distributed hydrological models. *Hydrology and Earth System Sciences*, 25(9), 5287–5313. <https://doi.org/10.5194/hess-25-5287-2021>
- Elliott, J., Deryng, D., Müller, C., Frieler, K., Konzmann, M., Gerten, D., et al. (2014). Constraints and potentials of future irrigation water availability on agricultural production under climate change. *Proceedings of the National Academy of Sciences*, 111(9), 3239–3244. <https://doi.org/10.1073/pnas.1222474110>
- 1180 Falkenmark, M., & Rockström, J. (2006). The New Blue and Green Water Paradigm: Breaking New Ground for Water Resources Planning and Management. *Journal of Water Resources Planning and Management*, 132(3), 129–132. [https://doi.org/10.1061/\(ASCE\)0733-9496\(2006\)132:3\(129\)](https://doi.org/10.1061/(ASCE)0733-9496(2006)132:3(129))
- Fan, Y., Chen, Y., He, Q., Li, W., & Wang, Y. (2016). Isotopic Characterization of River Waters and Water Source Identification in an Inland River, Central Asia. *Water*, 8(7), 286. <https://doi.org/10.3390/w8070286>
- 1185 Fekete, B. M., Vörösmarty, C. J., & Grabs, W. (2002). High-resolution fields of global runoff combining observed river discharge and simulated water balances: HIGH-RESOLUTION COMPOSITE RUNOFF FIELDS. *Global Biogeochemical Cycles*, 16(3), 15-1-15–10. <https://doi.org/10.1029/1999GB001254>
- Fekete, B. M., Gibson, J. J., Aggarwal, P., & Vörösmarty, C. J. (2006). Application of isotope tracers in continental scale hydrological modeling. *Journal of Hydrology*, 330(3–4), 444–456. <https://doi.org/10.1016/j.jhydrol.2006.04.029>
- 1190 Fischer, G., Nachtergaele, F., Prieler, S., van Velthuisen, H. T., Verelst, L., & Wiberg, D. (2008). Global Agro-ecological Zones Assessment for Agriculture (GAEZ 2008). IIASA, Laxenburg, Austria and FAO, Rome, Italy.
- Frenken, K. (Ed.). (2012). *Irrigation in Southern and Eastern Asia in figures: Aquastat survey, 2011*. Rome: Food and Agriculture of the United Nations.
- 1195 Gelaro, R., McCarty, W., Suárez, M. J., Todling, R., Molod, A., Takacs, L., et al. (2017). The Modern-Era Retrospective Analysis for Research and Applications, Version 2 (MERRA-2). *Journal of Climate*, 30(14), 5419–5454. <https://doi.org/10.1175/JCLI-D-16-0758.1>
- Ghassemi, F., & White, I. (2007). *Inter-basin water transfer: case studies from Australia, United States, Canada, China, and India*. Cambridge, UK ; New York: Cambridge University Press.
- 1200 Gleeson, T., Wada, Y., Bierkens, M. F. P., & van Beek, L. P. H. (2012). Water balance of global aquifers revealed by groundwater footprint. *Nature*, 488(7410), 197–200. <https://doi.org/10.1038/nature11295>
- Gleick, P. H., Pacific Institute for Studies in Development, Environment, and Security, & Stockholm Environment Institute (Eds.). (1993). *Water in crisis: a guide to the world's fresh water resources*. New York: Oxford University Press.



- 1205 Grafton, R. Q., Williams, J., Perry, C. J., Molle, F., Ringler, C., Steduto, P., et al. (2018). The paradox of irrigation efficiency. *Science*, 361(6404), 748–750. <https://doi.org/10.1126/science.aat9314>
- Grogan, D. S. (2016). GLOBAL AND REGIONAL ASSESSMENTS OF UNSUSTAINABLE GROUNDWATER USE IN IRRIGATED AGRICULTURE, 221.
- 1210 Grogan, D. S., Wisser, D., Prusevich, A., Lammers, R. B., & Frohling, S. (2017). The use and re-use of unsustainable groundwater for irrigation: a global budget. *Environmental Research Letters*, 12(3), 034017. <https://doi.org/10.1088/1748-9326/aa5fb2>
- Grogan, D. S., Burakowski, E. A., & Contosta, A. R. (2020). Snowmelt control on spring hydrology declines as the vernal window lengthens. *Environmental Research Letters*, 15(11), 114040. <https://doi.org/10.1088/1748-9326/abbd00>
- 1215 Grogan, Danielle S., Zhang, F., Prusevich, A., Lammers, R. B., Wisser, D., Glidden, S., et al. (2015). Quantifying the link between crop production and mined groundwater irrigation in China. *Science of The Total Environment*, 511, 161–175. <https://doi.org/10.1016/j.scitotenv.2014.11.076>
- Grogan, Danielle S., Wisser, D., Prusevich, A., Lammers, R. B., & Frohling, S. (2017). The use and re-use of unsustainable groundwater for irrigation: a global budget. *Environmental Research Letters*, 12(3), 034017. <https://doi.org/10.1088/1748-9326/aa5fb2>
- 1220 Groisman, P. Ya., Bulygina, O. N., Henebry, G. M., Speranskaya, N. A., Shiklomanov, A. I., Chen, Y., et al. (2020). Dry Land Belt of Northern Eurasia: Contemporary Environmental Changes. In G. Gutman, J. Chen, G. M. Henebry, & M. Kappas (Eds.), *Landscape Dynamics of Drylands across Greater Central Asia: People, Societies and Ecosystems* (Vol. 17, pp. 11–23). Cham: Springer International Publishing. [https://doi.org/10.1007/978-3-030-30742-4\\_2](https://doi.org/10.1007/978-3-030-30742-4_2)
- 1225 Haddeland, I., Heinke, J., Biemans, H., Eisner, S., Flörke, M., Hanasaki, N., et al. (2014). Global water resources affected by human interventions and climate change. *Proceedings of the National Academy of Sciences*, 111(9), 3251–3256. <https://doi.org/10.1073/pnas.1222475110>
- Haie, N., & Keller, A. A. (2008). Effective Efficiency as a Tool for Sustainable Water Resources Management <sup>1</sup>. *JAWRA Journal of the American Water Resources Association*, 44(4), 961–968. <https://doi.org/10.1111/j.1752-1688.2008.00194.x>
- 1230 Håkanson, L. (2005). The importance of lake morphometry and catchment characteristics in limnology – ranking based on statistical analyses. *Hydrobiologia*, 541(1), 117–137. <https://doi.org/10.1007/s10750-004-5032-7>
- Hanasaki, N., Kanae, S., Oki, T., Masuda, K., Motoya, K., Shirakawa, N., et al. (2008a). An integrated model for the assessment of global water resources – Part 1: Model description and input meteorological forcing. *Hydrology and Earth System Sciences*, 12(4), 1007–1025. <https://doi.org/10.5194/hess-12-1007-2008>
- 1235 Hanasaki, N., Kanae, S., Oki, T., Masuda, K., Motoya, K., Shirakawa, N., et al. (2008b). An integrated model for the assessment of global water resources – Part 2: Applications and assessments. *Hydrology and Earth System Sciences*, 12(4), 1027–1037. <https://doi.org/10.5194/hess-12-1027-2008>
- 1240 Hanasaki, Naota, Yoshikawa, S., Pokhrel, Y., & Kanae, S. (2018). A global hydrological simulation to specify the sources of water used by humans. *Hydrology and Earth System Sciences*, 22(1), 789–817. <https://doi.org/10.5194/hess-22-789-2018>
- Haqiqi, I., Grogan, D. S., Hertel, T. W., & Schlenker, W. (2020). *Quantifying the Impacts of Compound Extremes on Agriculture and Irrigation Water Demand* (preprint). Water Resources Management/Theory development. <https://doi.org/10.5194/hess-2020-275>
- 1245 Haqiqi, I., Grogan, D. S., Hertel, T. W., & Schlenker, W. (2021). Quantifying the impacts of compound extremes on agriculture. *Hydrology and Earth System Sciences*, 25(2), 551–564. <https://doi.org/10.5194/hess-25-551-2021>





- Hrachowitz, M., Savenije, H., Bogaard, T. A., Tetzlaff, D., & Soulsby, C. (2013). What can flux tracking teach us about water age distribution patterns and their temporal dynamics? *Hydrology and Earth System Sciences*, 17(2), 533–564. <https://doi.org/10.5194/hess-17-533-2013>
- 1250 Huang, T., Wollheim, W. M., & Jones, S. H. (2022). Removal of Fecal Indicator Bacteria by River Networks. *Water*, 14(4), 617. <https://doi.org/10.3390/w14040617>
- Huss, M., & Hock, R. (2015). A new model for global glacier change and sea-level rise. *Frontiers in Earth Science*, 3. <https://doi.org/10.3389/feart.2015.00054>
- 1255 Jägermeyr, J., Gerten, D., Heinke, J., Schaphoff, S., Kummu, M., & Lucht, W. (2015). Water savings potentials of irrigation systems: global simulation of processes and linkages. *Hydrol. Earth Syst. Sci.*, 19(7), 3073–3091. <https://doi.org/10.5194/hess-19-3073-2015>
- Jägermeyr, J., Gerten, D., Schaphoff, S., Heinke, J., Lucht, W., & Rockström, J. (2016). Integrated crop water management might sustainably halve the global food gap. *Environmental Research Letters*, 11(2), 025002. <https://doi.org/10.1088/1748-9326/11/2/025002>
- 1260 Kadiresan, K., & Khanal, P. R. (2018). Rethinking Irrigation for Global Food Security: Irrigation and food security. *Irrigation and Drainage*, 67(1), 8–11. <https://doi.org/10.1002/ird.2219>
- Konar, M., Hussein, Z., Hanasaki, N., Mauzerall, D. L., & Rodriguez-Iturbe, I. (2013). Virtual water trade flows and savings under climate change. *Hydrology and Earth System Sciences*, 17(8), 3219–3234. <https://doi.org/10.5194/hess-17-3219-2013>
- 1265 Konikow, L. F. (2011). Contribution of global groundwater depletion since 1900 to sea-level rise: GROUNDWATER DEPLETION. *Geophysical Research Letters*, 38(17), n/a-n/a. <https://doi.org/10.1029/2011GL048604>
- Kumar, S., Peterslidard, C., Tian, Y., Houser, P., Geiger, J., Olden, S., et al. (2006). Land information system: An interoperable framework for high resolution land surface modeling. *Environmental Modelling & Software*, 21(10), 1402–1415. <https://doi.org/10.1016/j.envsoft.2005.07.004>
- 1270 Lawrence, D. M., Fisher, R. A., Koven, C. D., Oleson, K. W., Swenson, S. C., Bonan, G., et al. (2019). The Community Land Model Version 5: Description of New Features, Benchmarking, and Impact of Forcing Uncertainty. *Journal of Advances in Modeling Earth Systems*, 11(12), 4245–4287. <https://doi.org/10.1029/2018MS001583>
- Lehner, B., Verdin, K., & Jarvis, A. (2008). New Global Hydrography Derived From Spaceborne Elevation Data. *Eos, Transactions American Geophysical Union*, 89(10), 93–94. <https://doi.org/10.1029/2008EO100001>
- 1275 Lehner, B., Liermann, C. R., Revenga, C., Vörösmarty, C., Fekete, B., Crouzet, P., et al. (2011). High-resolution mapping of the world's reservoirs and dams for sustainable river-flow management. *Frontiers in Ecology and the Environment*, 9(9), 494–502. <https://doi.org/10.1890/100125>
- Leopold, L. B., & Maddock, T. (1953). of Stream Channels and Some Physiographic Implications, 64.
- 1280 Liu, J., Hertel, T. W., Lammers, R. B., Prusevich, A., Baldos, U. L. C., Grogan, D. S., & Froelking, S. (2017). Achieving sustainable irrigation water withdrawals: global impacts on food security and land use. *Environmental Research Letters*, 12(10), 104009. <https://doi.org/10.1088/1748-9326/aa88db>
- Maidment, D. R. (Ed.). (1993). *Handbook of hydrology*. New York: McGraw-Hill.
- Mineau, M. M., Wollheim, W. M., & Stewart, R. J. (2015). An index to characterize the spatial distribution of land use within watersheds and implications for river network nutrient removal and export. *Geophysical Research Letters*, 42(16), 6688–6695. <https://doi.org/10.1002/2015GL064965>



- 1285 Mishra, S. K., Veselka, T. D., Prusevich, A. A., Grogan, D. S., Lammers, R. B., Rounce, D. R., et al. (2020). Differential Impact of Climate Change on the Hydropower Economics of Two River Basins in High Mountain Asia. *Frontiers in Environmental Science*, 8, 26. <https://doi.org/10.3389/fenvs.2020.00026>
- Mulholland, P. J., Helton, A. M., Poole, G. C., Hall, R. O., Hamilton, S. K., Peterson, B. J., et al. (2008). Stream denitrification across biomes and its response to anthropogenic nitrate loading. *Nature*, 452(7184), 202–205. <https://doi.org/10.1038/nature06686>
- 1290 Niswonger, R. G., Morway, E. D., Triana, E., & Huntington, J. L. (2017). Managed aquifer recharge through off-season irrigation in agricultural regions. *Water Resources Research*, 53(8), 6970–6992. <https://doi.org/10.1002/2017WR020458>
- 1295 Park, C. C. (1977). World-wide variations in hydraulic geometry exponents of stream channels: An analysis and some observations. *Journal of Hydrology*, 33(1–2), 133–146. [https://doi.org/10.1016/0022-1694\(77\)90103-2](https://doi.org/10.1016/0022-1694(77)90103-2)
- Penman, H.L. (1948). Natural evaporation from open water, bare soil and grass, 27.
- Plummer, L. N., Rupert, M. G., Busenberg, E., & Schlosser, P. (2000). Age of Irrigation Water in Ground Water from the Eastern Snake River Plain Aquifer, South-Central Idaho. *Ground Water*, 38(2), 264–283. <https://doi.org/10.1111/j.1745-6584.2000.tb00338.x>
- 1300 Pokhrel, Y., Hanasaki, N., Koirala, S., Cho, J., Yeh, P. J.-F., Kim, H., et al. (2012). Incorporating Anthropogenic Water Regulation Modules into a Land Surface Model. *Journal of Hydrometeorology*, 13(1), 255–269. <https://doi.org/10.1175/JHM-D-11-013.1>
- Pokhrel, Y. N., Hanasaki, N., Yeh, P. J.-F., Yamada, T. J., Kanae, S., & Oki, T. (2012). Model estimates of sea-level change due to anthropogenic impacts on terrestrial water storage. *Nature Geoscience*, 5(6), 389–392. <https://doi.org/10.1038/ngeo1476>
- 1305 Portmann, F. T., Siebert, S., & Döll, P. (2010). MIRCA2000-Global monthly irrigated and rainfed crop areas around the year 2000: A new high-resolution data set for agricultural and hydrological modeling: MONTHLY IRRIGATED AND RAINFED CROP AREAS. *Global Biogeochemical Cycles*, 24(1), n/a-n/a. <https://doi.org/10.1029/2008GB003435>
- 1310 Prusevich, A., Lammers, R., & Grogan, D. (2021). High Mountain Asia Rasterized PyGEM Glacier Projections with RCP Scenarios [Data set]. NASA National Snow and Ice Data Center DAAC. <https://doi.org/10.5067/H118TCMSUH3Q>
- Rajib, A., Golden, H. E., Lane, C. R., & Wu, Q. (2020). Surface Depression and Wetland Water Storage Improves Major River Basin Hydrologic Predictions. *Water Resources Research*, 56(7). <https://doi.org/10.1029/2019WR026561>
- 1315 Rawlins, M. A., Lammers, R. B., Frohling, S., Fekete, B. M., & Vorosmarty, C. J. (2003). Simulating pan-Arctic runoff with a macro-scale terrestrial water balance model. *Hydrological Processes*, 17(13), 2521–2539. <https://doi.org/10.1002/hyp.1271>
- Rawlins, M. A., McDonald, K. C., Frohling, S., Lammers, R. B., Fahnestock, M., Kimball, J. S., & Vörösmarty, C. J. (2005). Remote sensing of snow thaw at the pan-Arctic scale using the SeaWinds scatterometer. *Journal of Hydrology*, 312(1–4), 294–311. <https://doi.org/10.1016/j.jhydrol.2004.12.018>
- 1320 Rawlins, M. A., Frohling, S., Lammers, R. B., & Vörösmarty, C. J. (2006). Effects of Uncertainty in Climate Inputs on Simulated Evapotranspiration and Runoff in the Western Arctic. *Earth Interactions*, 10(18), 1–18. <https://doi.org/10.1175/EI182.1>
- Rawlins, M. A., Willmott, C. J., Shiklomanov, A., Linder, E., Frohling, S., Lammers, R. B., & Vörösmarty, C. J. (2006). Evaluation of trends in derived snowfall and rainfall across Eurasia and linkages with discharge to the Arctic Ocean. *Geophysical Research Letters*, 33(7), L07403. <https://doi.org/10.1029/2005GL025231>



- 1325 Rawlins, M. A., Cai, L., Stuefer, S. L., & Nicolsky, D. (2019). Changing characteristics of runoff and freshwater export from watersheds draining northern Alaska. *The Cryosphere*, 13(12), 3337–3352. <https://doi.org/10.5194/tc-13-3337-2019>
- Rienecker, M. M., Suarez, M. J., Gelaro, R., Todling, R., Bacmeister, J., Liu, E., et al. (2011). MERRA: NASA’s Modern-Era Retrospective Analysis for Research and Applications. *Journal of Climate*, 24(14), 3624–3648. <https://doi.org/10.1175/JCLI-D-11-00015.1>
- 1330 Rimsaite, R. (2021). How Well Do U.S. Western Water Markets Convey Economic Information? *Land Economics*, 16.
- Rosegrant, M. W., & Cai, X. (2002). Global Water Demand and Supply Projections: Part 2. Results and Prospects to 2025. *Water International*, 27(2), 170–182. <https://doi.org/10.1080/02508060208686990>
- Rost, S., Gerten, D., Bondeau, A., Lucht, W., Rohwer, J., & Schaphoff, S. (2008). Agricultural green and blue water consumption and its influence on the global water system: GLOBAL WATER USE IN AGRICULTURE. *Water Resources Research*, 44(9). <https://doi.org/10.1029/2007WR006331>
- 1335 Rougé, C., Reed, P. M., Grogan, D. S., Zuidema, S., Prusevich, A., Glidden, S., et al. (2021). Coordination and control – limits in standard representations of multi-reservoir operations in hydrological modeling. *Hydrology and Earth System Sciences*, 25(3), 1365–1388. <https://doi.org/10.5194/hess-25-1365-2021>
- Rounce, D. R., Hock, R., & Shean, D. E. (2020). Glacier Mass Change in High Mountain Asia Through 2100 Using the Open-Source Python Glacier Evolution Model (PyGEM). *Frontiers in Earth Science*, 7, 331. <https://doi.org/10.3389/feart.2019.00331>
- 1340 Rounce, D. R., Khurana, T., Short, M. B., Hock, R., Shean, D. E., & Brinkerhoff, D. J. (2020). Quantifying parameter uncertainty in a large-scale glacier evolution model using Bayesian inference: application to High Mountain Asia. *Journal of Glaciology*, 66(256), 175–187. <https://doi.org/10.1017/jog.2019.91>
- 1345 Sadegh, M., & Vrugt, J. A. (2013). Bridging the gap between GLUE and formal statistical approaches: approximate Bayesian computation. *Hydrology and Earth System Sciences*, 17(12), 4831–4850. <https://doi.org/10.5194/hess-17-4831-2013>
- Saha, S., Moorthi, S., Wu, X., Wang, J., Nadiga, S., Tripp, P., et al. (2014). The NCEP Climate Forecast System Version 2. *Journal of Climate*, 27(6), 2185–2208. <https://doi.org/10.1175/JCLI-D-12-00823.1>
- 1350 Samal, N. R., Wollheim, W. M., Zuidema, S., Stewart, R. J., Zhou, Z., Mineau, M. M., et al. (2017a). A coupled terrestrial and aquatic biogeophysical model of the Upper Merrimack River watershed, New Hampshire, to inform ecosystem services evaluation and management under climate and land-cover change. *Ecology and Society*, 22(4), art18. <https://doi.org/10.5751/ES-09662-220418>
- 1355 Samal, N. R., Wollheim, W., Zuidema, S., Stewart, R., Zhou, Z., Mineau, M., et al. (2017b). A coupled terrestrial and aquatic biogeophysical model of the Upper Merrimack River watershed, New Hampshire, to inform ecosystem services evaluation and management under climate and land-cover change. *Ecology and Society*, 22(4), 18. <https://doi.org/10.5751/ES-09662-220418>
- Schewe, J., Heinke, J., Gerten, D., Haddeland, I., Arnell, N. W., Clark, D. B., et al. (2014). Multimodel assessment of water scarcity under climate change. *Proceedings of the National Academy of Sciences*, 111(9), 3245–3250. <https://doi.org/10.1073/pnas.1222460110>
- 1360 Shiklomanov, A. I., Lammers, R. B., Lettenmaier, D. P., Polischuk, Y. M., Savichev, O. G., Smith, L. C., & Chernokulsky, A. V. (2013). Hydrological Changes: Historical Analysis, Contemporary Status, and Future Projections. In P. Ya. Groisman & G. Gutman (Eds.), *Regional Environmental Changes in Siberia and Their Global Consequences* (pp. 111–154). Dordrecht: Springer Netherlands. [https://doi.org/10.1007/978-94-007-4569-8\\_4](https://doi.org/10.1007/978-94-007-4569-8_4)



- 1365 Siebert, S., & Döll, P. (2010). Quantifying blue and green virtual water contents in global crop production as well as potential production losses without irrigation. *Journal of Hydrology*, 384(3–4), 198–217. <https://doi.org/10.1016/j.jhydrol.2009.07.031>
- Simon, D. (2018). *The Impact of Dams on Floods and Nitrogen Flux in the Lamprey River Watershed, NH* (M.S.). University of New Hampshire, United States -- New Hampshire. Retrieved from <https://search.proquest.com/pqdtlocal1006039/docview/2176393164/abstract/DAB49D5D4A354CF2PQ/1>
- 1370 St Amour, N. A., Gibson, J. J., Edwards, T. W. D., Prowse, T. D., & Pietroniro, A. (2005). Isotopic time-series partitioning of streamflow components in wetland-dominated catchments, lower Liard River basin, Northwest Territories, Canada. *Hydrological Processes*, 19(17), 3357–3381. <https://doi.org/10.1002/hyp.5975>
- 1375 Stewart, R. J., Wollheim, W. M., Gooseff, M. N., Briggs, M. A., Jacobs, J. M., Peterson, B. J., & Hopkinson, C. S. (2011a). Separation of river network-scale nitrogen removal among the main channel and two transient storage compartments. *Water Resources Research*, 47(1). <https://doi.org/10.1029/2010WR009896>
- 1380 Stewart, R. J., Wollheim, W. M., Gooseff, M. N., Briggs, M. A., Jacobs, J. M., Peterson, B. J., & Hopkinson, C. S. (2011b). Separation of river network-scale nitrogen removal among the main channel and two transient storage compartments: TRANSIENT STORAGE AND NETWORK DIN REMOVAL. *Water Resources Research*, 47(10). <https://doi.org/10.1029/2010WR009896>
- Stewart, R. J., Wollheim, W. M., Miara, A., Vörösmarty, C. J., Fekete, B., Lammers, R. B., & Rosenzweig, B. (2013). Horizontal cooling towers: riverine ecosystem services and the fate of thermoelectric heat in the contemporary Northeast US. *Environmental Research Letters*, 8(2), 025010. <https://doi.org/10.1088/1748-9326/8/2/025010>
- 1385 Sulser, T. B., Ringler, C., Zhu, T., Msangi, S., Bryan, E., & Rosegrant, M. W. (2010). Green and blue water accounting in the Ganges and Nile basins: Implications for food and agricultural policy. *Journal of Hydrology*, 384(3–4), 276–291. <https://doi.org/10.1016/j.jhydrol.2009.10.003>
- Sutanudjaja, E. H., van Beek, R., Wanders, N., Wada, Y., Bosmans, J. H. C., Drost, N., et al. (2018). PCR-GLOBWB 2: a 5 arcmin global hydrological and water resources model. *Geoscientific Model Development*, 11(6), 2429–2453. <https://doi.org/10.5194/gmd-11-2429-2018>
- 1390 Telteu, C.-E., Müller Schmied, H., Thiery, W., Leng, G., Burek, P., Liu, X., et al. (2021). Understanding each other's models: an introduction and a standard representation of 16 global water models to support intercomparison, improvement, and communication. *Geoscientific Model Development*, 14(6), 3843–3878. <https://doi.org/10.5194/gmd-14-3843-2021>
- 1395 Tran, D., Kovacs, K., & Wallander, S. (2019). Long run optimization of landscape level irrigation through managed aquifer recharge or expanded surface reservoirs. *Journal of Hydrology*, 579, 124220. <https://doi.org/10.1016/j.jhydrol.2019.124220>
- Turner, S. W. D., Hejazi, M., Yonkofski, C., Kim, S. H., & Kyle, P. (2019). Influence of Groundwater Extraction Costs and Resource Depletion Limits on Simulated Global Nonrenewable Water Withdrawals Over the Twenty-First Century. *Earth's Future*, 7(2), 123–135. <https://doi.org/10.1029/2018EF001105>
- 1400 Van Kirk, R. W., Contor, B. A., Morrisett, C. N., Null, S. E., & Loibman, A. S. (2020). Potential for Managed Aquifer Recharge to Enhance Fish Habitat in a Regulated River. *Water*, 12(3), 673. <https://doi.org/10.3390/w12030673>
- Vörösmarty, C. J., Moore, B., Grace, A. L., Gildea, M. P., Melillo, J. M., Peterson, B. J., et al. (1989). Continental scale models of water balance and fluvial transport: An application to South America. *Global Biogeochemical Cycles*, 3(3), 241–265. <https://doi.org/10.1029/GB003i003p00241>



- 1405 Vörösmarty, C. J., Federer, C. A., & Schloss, A. L. (1998). Potential evaporation functions compared on US watersheds: Possible implications for global-scale water balance and terrestrial ecosystem modeling. *Journal of Hydrology*, 207(3–4), 147–169. [https://doi.org/10.1016/S0022-1694\(98\)00109-7](https://doi.org/10.1016/S0022-1694(98)00109-7)
- Vörösmarty, C. J., Fekete, B. M., Meybeck, M., & Lammers, R. B. (2000). Geomorphometric attributes of the global system of rivers at 30-minute spatial resolution. *Journal of Hydrology*, 237(1–2), 17–39. [https://doi.org/10.1016/S0022-1694\(00\)00282-1](https://doi.org/10.1016/S0022-1694(00)00282-1)
- 1410 Vörösmarty, C. J., Green, P., Salisbury, J., & Lammers, R. B. (2000). Global Water Resources: Vulnerability from Climate Change and Population Growth. *Science*, 289(5477), 284–288. <https://doi.org/10.1126/science.289.5477.284>
- Vörösmarty, C. J., Douglas, E. M., Green, P. A., & Revenga, C. (2005). Geospatial Indicators of Emerging Water Stress: An Application to Africa. *AMBIO: A Journal of the Human Environment*, 34(3), 230–236. <https://doi.org/10.1579/0044-7447-34.3.230>
- 1415 Vörösmarty, C. J., McIntyre, P. B., Gessner, M. O., Dudgeon, D., Prusevich, A., Green, P., et al. (2010). Global threats to human water security and river biodiversity. *Nature*, 467(7315), 555–561. <https://doi.org/10.1038/nature09440>
- Wada, Y., van Beek, L. P. H., & Bierkens, M. F. P. (2011). Modelling global water stress of the recent past: on the relative importance of trends in water demand and climate variability. *Hydrology and Earth System Sciences*, 15(12), 3785–3808. <https://doi.org/10.5194/hess-15-3785-2011>
- 1420 Wada, Y., Wisser, D., & Bierkens, M. F. P. (2014). Global modeling of withdrawal, allocation and consumptive use of surface water and groundwater resources. *Earth System Dynamics*, 5(1), 15–40. <https://doi.org/10.5194/esd-5-15-2014>
- Wada, Yoshihide, van Beek, L. P. H., & Bierkens, M. F. P. (2012). Nonsustainable groundwater sustaining irrigation: A global assessment: NONSUSTAINABLE GROUNDWATER SUSTAINING IRRIGATION. *Water Resources Research*, 48(6). <https://doi.org/10.1029/2011WR010562>
- Wada, Yoshihide, Lo, M.-H., Yeh, P. J.-F., Reager, J. T., Famiglietti, J. S., Wu, R.-J., & Tseng, Y.-H. (2016). Fate of water pumped from underground and contributions to sea-level rise. *Nature Climate Change*, 6(8), 777–780. <https://doi.org/10.1038/nclimate3001>
- 1430 Webster, M., Fisher-Vanden, K., Kumar, V., Lammers, R. B., & Perla, J. (2022). Integrated hydrological, power system and economic modelling of climate impacts on electricity demand and cost. *Nature Energy*. <https://doi.org/10.1038/s41560-021-00958-8>
- Weiler, M., Seibert, J., & Stahl, K. (2018). Magic components-why quantifying rain, snowmelt, and icemelt in river discharge is not easy. *Hydrological Processes*, 32(1), 160–166. <https://doi.org/10.1002/hyp.11361>
- 1435 Willmott, C. J. (1981). ON THE VALIDATION OF MODELS. *Physical Geography*, 2(2), 184–194. <https://doi.org/10.1080/02723646.1981.10642213>
- Willmott, C. J., Rowe, C. M., & Mintz, Y. (1985). Climatology of the terrestrial seasonal water cycle. *Journal of Climatology*, 5(6), 589–606. <https://doi.org/10.1002/joc.3370050602>
- 1440 Wisser, D., Froliking, S., Douglas, E. M., Fekete, B. M., Vörösmarty, C. J., & Schumann, A. H. (2008). Global irrigation water demand: Variability and uncertainties arising from agricultural and climate data sets. *Geophysical Research Letters*, 35(24), L24408. <https://doi.org/10.1029/2008GL035296>
- Wisser, D., Fekete, B. M., Vorosmarty, C. J., & Schumann, A. H. (2010a). Reconstructing 20th century global hydrography: a contribution to the Global Terrestrial Network- Hydrology (GTN-H). *Hydrol. Earth Syst. Sci.*, 24.
- 1445 Wisser, D., Fekete, B. M., Vorosmarty, C. J., & Schumann, A. H. (2010b). Reconstructing 20th century global hydrography: a contribution to the Global Terrestrial Network- Hydrology (GTN-H). *Hydrol. Earth Syst. Sci.*, 24.



- Wisser, D., Frohking, S., Douglas, E. M., Fekete, B. M., Schumann, A. H., & Vörösmarty, C. J. (2010). The significance of local water resources captured in small reservoirs for crop production – A global-scale analysis. *Journal of Hydrology*, 384(3–4), 264–275. <https://doi.org/10.1016/j.jhydrol.2009.07.032>
- 1450 Wit, M. J. M. de. (2001). Nutrient fluxes at the river basin scale. I: the PolFlow model. *Hydrological Processes*, 15(5), 743–759. <https://doi.org/10.1002/hyp.175>
- Wollheim, W., Peterson, B. J., Thomas, S. M., Hopkinson, C. H., & Vörösmarty, C. J. (2008). Dynamics of N removal over annual time periods in a suburban river network. *Journal of Geophysical Research*, 113(G3), G03038. <https://doi.org/10.1029/2007JG000660>
- 1455 Wollheim, W., Vörösmarty, C. J., Bouwman, A. F., Green, P., Harrison, J., Linder, E., et al. (2008). Global N removal by freshwater aquatic systems using a spatially distributed, within-basin approach: FRAMES-N-GLOBAL AQUATIC N CYCLE. *Global Biogeochemical Cycles*, 22(2), n/a-n/a. <https://doi.org/10.1029/2007GB002963>
- Wollheim, W., Stewart, R. J., Aiken, G. R., Butler, K. D., Morse, N. B., & Salisbury, J. (2015). Removal of terrestrial DOC in aquatic ecosystems of a temperate river network. *Geophysical Research Letters*, 42(16), 6671–6679. <https://doi.org/10.1002/2015GL064647>
- 1460 Wollheim, WM, Peterson, B. J., Thomas, S. M., Hopkinson, C. S., & Vorosmarty, C. J. (2008). Dynamics of N removal over annual time periods in a suburban river network.
- Wollheim, WM, Harms, T. K., Peterson, B. J., Morkeski, K., Hopkinson, C. S., Stewart, R. J., et al. (2014). Nitrate uptake dynamics of surface transient storage in stream channels and fluvial wetlands. *Biogeochemistry*, 120(1–3), 239–257. <https://doi.org/10.1007/s10533-014-9993-y>
- 1465 Yamazaki, D., Kanae, S., Kim, H., & Oki, T. (2011). A physically based description of floodplain inundation dynamics in a global river routing model: FLOODPLAIN INUNDATION DYNAMICS. *Water Resources Research*, 47(4). <https://doi.org/10.1029/2010WR009726>
- Yamazaki, D., Ikeshima, D., Sosa, J., Bates, P. D., Allen, G. H., & Pavelsky, T. M. (2019). MERIT Hydro: A High-Resolution Global Hydrography Map Based on Latest Topography Dataset. *Water Resources Research*, 55(6), 5053–5073. <https://doi.org/10.1029/2019WR024873>
- 1470 Yang, Y., Donohue, R. J., & McVicar, T. R. (2016). Global estimation of effective plant rooting depth: Implications for hydrological modeling: GLOBAL HYDROLOGICAL EFFECTIVE ROOTING DEPTH. *Water Resources Research*, 52(10), 8260–8276. <https://doi.org/10.1002/2016WR019392>
- 1475 Zaveri, E., Grogan, D. S., Fisher-Vanden, K., Frohking, S., Lammers, R. B., Wrenn, D. H., et al. (2016). Invisible water, visible impact: groundwater use and Indian agriculture under climate change. *Environmental Research Letters*, 11(8), 084005. <https://doi.org/10.1088/1748-9326/11/8/084005>
- Zeitoun, M., & Mirumachi, N. (2008). Transboundary water interaction I: reconsidering conflict and cooperation. *International Environmental Agreements: Politics, Law and Economics*, 8(4), 297–316. <https://doi.org/10.1007/s10784-008-9083-5>
- 1480 Zuidema, S., & Morrison, R. (2020). Hydrologically Consistent Dams Database (version 2.0) [Data set]. Harvard Dataverse. <https://doi.org/10.7910/DVN/5YBWWI>
- Zuidema, S., Wollheim, W. M., Mineau, M. M., Green, M. B., & Stewart, R. J. (2018). Controls of Chloride Loading and Impairment at the River Network Scale in New England. *Journal of Environmental Quality*, 47(4), 839–847. <https://doi.org/10.2134/jeq2017.11.0418>
- 1485 Zuidema, S., Grogan, D., Prusevich, A., Lammers, R., Gilmore, S., & Williams, P. (2020). Interplay of changing irrigation technologies and water reuse: Example from the Upper Snake River Basin, Idaho, USA. <https://doi.org/10.5194/hess-2020-135>